FACULTY OF ENGINEERING AND ARCHITECTURE

Computational Modelling of Dorsal Root Ganglion Stimulation for Pain Relief

Sebastiaan Priem
Student number: 01406639

Supervisors: Prof. dr. ir. Emmeric Tanghe, Prof. ir. Vincent Keereman
Counsellors: Tom Van de Steene, Thomas Tarnaud

Master's dissertation submitted in order to obtain the academic degree of
Master of Science in Biomedical Engineering

Academic year 2020-2021

GHENT UNIVERSITY

FACULTY OF ENGINEERING AND ARCHITECTURE

Computational Modelling of Dorsal Root Ganglion Stimulation for Pain Relief

Sebastiaan Priem
Student number: 01406639

Supervisors: Prof. dr. ir. Emmeric Tanghe, Prof. ir. Vincent Keereman
Counsellors: Tom Van de Steene, Thomas Tarnaud

Master's dissertation submitted in order to obtain the academic degree of
Master of Science in Biomedical Engineering

Academic year 2020-2021

GHENT UNIVERSITY

Acknowledgments

First of all I would like to thank my counsellors ir. Tom Van de Steene and dr. ir. Thomas Tarnaud for always being available and guiding me through the process of writing this thesis. I would also like to thank my promotor prof. dr. ir. Emmeric Tanghe and my co-promotor prof. ir. Vincent Keereman for making it possible to work on this interesting subject for my final master dissertation as an engineering student. I would also like to express my gratitude to the WAVES research group for enabling me to work with the software that makes it possible to conduct my research. Finally I would like to thank my family for funding my studies and supporting me along the way.

Sebastiaan Priem

May 2021

Abstract

In this master dissertation the behavior of Aβ and C fibers when performing dorsal root ganglion stimulation (DRGS) is studied to optimise this promising technique for pain relief.

To determine the behavior of these nerve fibers a computational model of the dorsal root ganglion (DRG) is constructed and simulations are performed using these models to further study the dorsal root ganglion stimulation technique. The following parameters are studied: cathodal and anodal stimulation, influence of the modulating pulse width and type, influence of the nerve fiber diameters and influence of varying positions of the nerve fibers within the DRG. In addition to this, a nerve bundle is studied to determine the percentage of activation by dorsal root ganglion stimulation and subsequently the range in which the electrodes should be implanted.

The model showed that Aβ fibers were effectively stimulated by dorsal root ganglion stimulation. Subsequently the most efficient way to stimulate these fibers was through monophasic stimulation using a pulse width of 0.3 ms. Finally the model showed that the electrode shaft should be implanted within the range of 3.65 - 6.75 mm center to center distance between the active electrode and the DRG. In contrast to Aβ fibers, C fibers were not stimulated within clinical ranges according to this model.

Keywords: dorsal root ganglion stimulation, chronic pain, neuromodulation, computational modelling, electric stimulation

Computational Modelling of Dorsal Root Ganglion Stimulation for Pain Relief

Sebastiaan Priem

Supervisors: Prof. dr. ir. Emmeric Tanghe, Prof. ir. Vincent Keereman
Counsellors: Ir. Tom Van De Steene, Dr. ir. Thomas Tarnaud

Abstract—**In this master dissertation the behaviour of Aβ and C fibers when exposed to an electrical field generated by dorsal root ganglion stimulation is analyzed. To study this behaviour a cylindrical model is created to mimic the environment of the dorsal root ganglion and surrounding structures. This model also includes electrodes from which the electrical field is generated as would be done in dorsal root ganglion stimulation. Optimization of this technique includes studying the influence on the excitation thresholds, times of spike and location of the first spike of the following parameters: anodic versus cathodic stimulation, modulating pulse width and type, nerve fiber diameter and varying positions of the nerve fibers within the model. A nerve fiber bundle is also stimulated to determine the range in which the electrodes should be implanted.**

Keywords—**chronic pain, computational modelling, electric stimulation, neuromodulation**

I. Introduction

The dorsal root ganglion (DRG) is a bilateral structure located within the neuroforamen which exists at every section of the spine as shown in Figure 1. The DRG is an extension of the dorsal root containing a variation of nerve fibers including: C fibers, high-threshold Aβ nociceptors and Aδ fibers [1]. DRG neurons are pseudo-unipolar meaning that the nerve fibers consist of an axon that bifurcates into two branches that travel to the perihperal nervous system (PNS) and to the central nervous system (CNS). By means of magnetic resonance imaging (MRI) and studies on cadavers the locations of dorsal root ganglia are determined [1]. These locations are shown on the right side of Figure 1. The main function of the DRG is the transmission of sensory messages from receptors such as thermoreceptors, nociceptors, proprioceptors and chemoreceptors to the CNS [2].

Dorsal root ganglion stimulation (DRGS) is used to relief patients of chronic pain. Alternative treatments are drug related treatments (e.g. analgesics), deep brain stimulation (DBS), spinal cord stimulation (SCS), etc [3]. Several limitations occur regarding spinal cord stimulation. Due to the anatomy of the spinal cord certain regions are difficult to reach by conventional SCS (e.g. feet, bladder) [4]. Also a high amount of cerebrospinal fluid (CSF) is present around the spinal cord causing occasional shuntig of the current away from the intended regions [5]. In addition to this the leads used in SCS are susceptible to positional changes over time (e.g. when the patient is aging and experiences postural changes) [6]. These limitations can result in less pain relief when using SCS.

S. Priem is a master student biomedical engineering, Ghent University (UGent), Gent, Belgium. E-mail: Sebastiaan.Priem@Ugent.be .

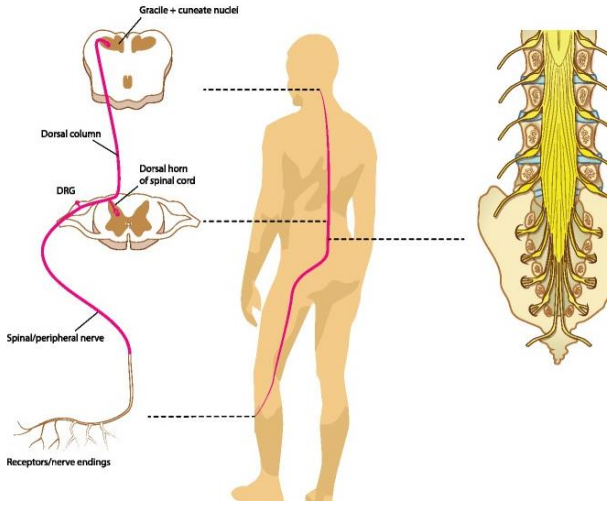

Figure 1 – Expansion of a primary sensory neuron, position of the dorsal root ganglion and cross-section of the spinal cord (left). Position of the dorsal root ganglia inside the lumbar and sacral spine (right) [1].

In DRGS a cylindrical electrode is implanted into the intraforaminal space above the DRG [7]. The intraforaminal space is compact and there are no large amounts of CSF present, resulting in less potitional changes of the leads in contrast to SCS [7]. Another benefit of DRGS is that it innervates one single dermatome, consequently regions that were hard to reach using SCS can be reached using DRGS [7].

II. Methods

The model used in this master dissertation is created in the software Sim4Life. This software provides a programming environment in which anatomical models can be made, simulations can be performed and results can be analyzed.

A. The DRG model

The model that is made, shown in Figure 2 is based on the finite element model of a human L5 DRG created by Graham et al. [7]. This model consists of the DRG surrounded by dural covering, intraforaminal tissue, bone and the general thorax. In addition to this the spinal and peripheral nerve root are also included. Finally an electrode shaft with the active electrode right above the DRG surrounded by an encapsulation layer is

added. The coordinate system is visible in the left corner with the X-axis in red, the Y-axis in green and the Z-axis in blue.

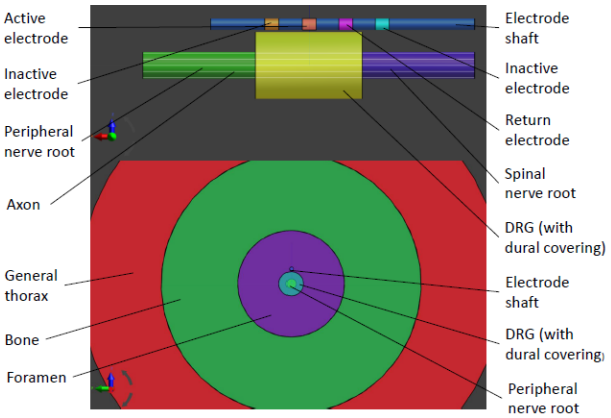

Figure 2 – The constructed model used in this thesis of a human L5 DRG with annotation of all elements.

B. *Modelling Aβ and C fibers*

To model the thick myelinated Aβ fibers the Spatially Extended Nonlinear Node or SENN model is used [8]. This model is a compromise between a simple single-node and a node-plus-myelin model. The SENN model is based on the equivalent electrical circuit of a myelinated fiber shown in Figure 3.

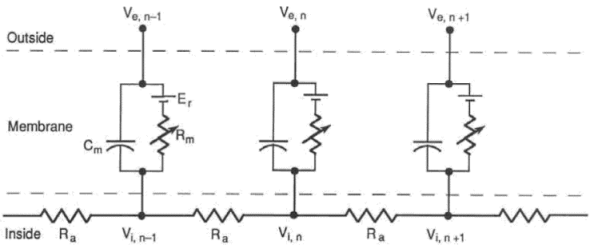

Figure 3 – The equivalent electrical circuit of a myelinated fiber [9].

The membrane consists of a capacitance C_m, resistance R_m and a potential source E_r. This source is added to maintain the resting potential of the membrane. The different circuits are connected through a resistance R_a representing the axoplasmic fluid. In the SENN model each ionic species has a different conductance. The different parameters for Aβ fibers used in this thesis can be found in Table 1.

Table 1 – SENN parameter values used to model Aβ fibers

Parameter	Value
Fiber diameter	7.3 µm
Axon diameter at node	5.11 µm
Nodal gap	2.5 µm
Axoplasmic resistivity	100 Ωcm
External medium resistivity	300 Ωcm
Membrane capacity	2 µF/cm²
Membrane conductivity	30.4 mS/cm²
Internodal distance	730 µm

Not only the behaviour of Aβ fibers is studied in this master dissertation, but also the behaviour of thin unmyelinated C fibers. To model these C fibers the Sundt model is used [10]. This model includes voltage-gated Na^+ channels and delayed rectifier K^+ channels. The parameter values used to model the C fibers are shown in Table 2.

Table 2 – Sundt parameter values used to model C fibers

Parameter	Value
Fiber diameter	0.8 µm
Axon diameter at node	0.8 µm
Section length	50 µm
Specific membrane resistivity	10000 Ωcm²
Axial resistance	100 Ωcm

C. *Activating threshold*

One of the most important parameters that has to be determined is the activation threshold. This is done by setting a boundary Dirichlet condition of 1 V (or -1 V depending on whether the electrode needs to be an anode or a cathode) on the active electrode and a boundary Dirichlet condition of 0V on the return electrode. When running the simulation a titration factor can be calculated. This factor has to multiplied with the modulating pulse and the external potential to find the activation threshold voltage. To derive the current from this threshold voltage the built-in flux evaluator is used. The flux evaluator works by computing the flux of the current vector field through a surface mesh. This computation directly gives the excitation threshold current.

D. *Grid study*

To accurately evaluate the electrical simulations performed with the model a grid study has to be conducted. This is done by decreasing the max step value in the grid settings to increase the grid resolution. A downside of increasing the grid size is that more computational power is needed to perform the simulations and consequently the simulation time will increase. To get a suitable grid, a grid mask is constructed around the active and return electrode and around the nerve fibers. A value of 1 V is applied to the active electrode and a value of 0 V to the return electrode. The max step of the total grid and the grid masks are then decreased until the titration factor did not change anymore.

E. *Automation of analysis*

Manually performing the modelling, simulations and analysis is very time consuming therefore a Python and two Matlab scripts are written. The python script constructs the model, performs the simulation and returns the analysis in a useable format (e.g. excel data and Matlab files). The first Matlab script, called Activating_Function.m, processes the electromagnetic field data (EM.mat) and plots the extracellular potential, the first derivative of this potential and the second derivative or activating function versus path along the axon. The axon is positioned along the X-axis which is directed to the right. This last one is particularly interesting because it gives the user an estimation of where de- and hyperpolarization will happen. The second Matlab script, called Membrane_Potential.m, plots the membrane potential versus path along the axon for different time stamps. The time stamps that are chosen are adaptable but interesting is to look at the

membrane potential right before stimulation, during stimulation and after stimulation. This can subsequently be compared to the activating function.

III. Results and Discussion

Initially the excitation thresholds are calculated for Aβ fibers in cathodal and anodal stimulations. Cathodal stimulations are defined by putting a Dirichlet boundary condition of -1 V on the active electrode (cathode) and 0 V on the return electrode (anode). Subsequently, the same simulations are done for C fibers. Thereafter the activating functions and corresponding membrane potentials are plotted. Next the influence of different parameters on the behaviour of these nerve fibers is examined (axon location, pulse width and type, axon diameter). Finally a bundle of nerve fibers is stimulated to determine the influence of the distance between the electrode shaft and the DRG on the percentage of activated neurons.

A. *Stimulation of Aβ fibers*

The activating functions ($f\frac{\partial^2 V_e}{\partial l^2}$, with l the path along the axon) for the Aβ fiber located in the center of the DRG for cathodal (A) and anodal (B) stimulation are shown in Figure 4.

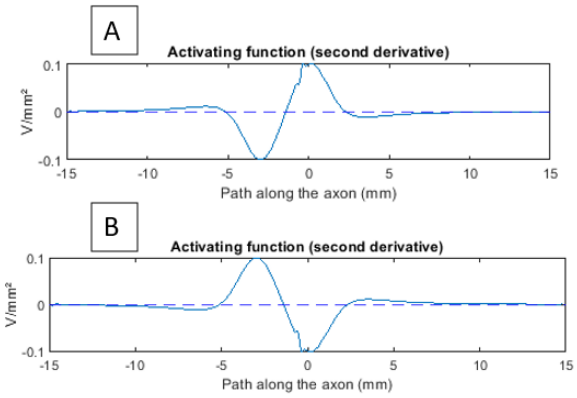

Figure 4 – Activating functions of the Aβ fiber positioned in the center of the DRG stimulated by cathodal (A) and anodal (B) stimulation.

Note that these are actually superpositions of activating functions. E.g. in the activating function for cathodal stimulation a high positive peak occurs at the 0 mm point. This is due to the high positive peak coming from the cathode and the small positive bump coming from the anode. The same conclusion can be made for the anodal activating function as this is a mirroring of the cathodal activating function around the X-axis. This is due to the fact that the anode and cathode are now switched.

To see if the predictions of the activating functions are correct the membrane potentials are plotted versus the path along the axon. These membrane potential plots can be seen in Figure 5 and are in accordance with the activating function.

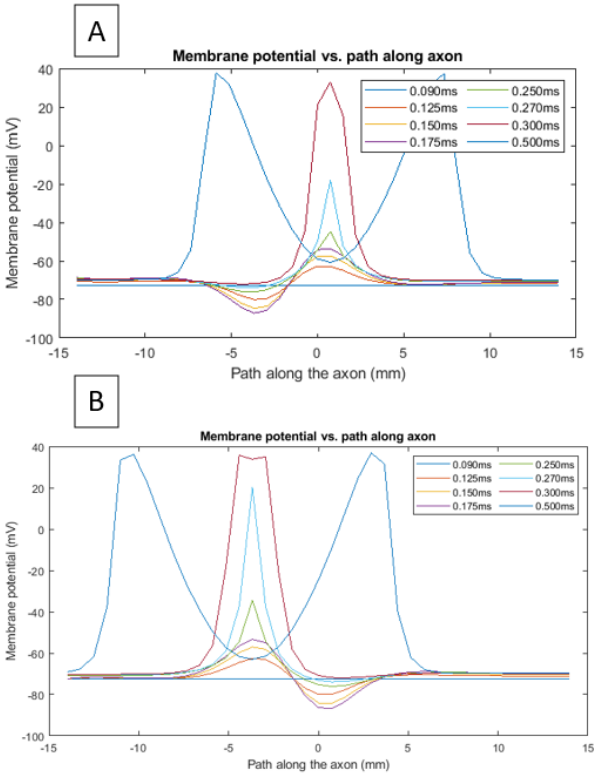

Figure 5 – Membrane potential plots of Aβ fibers when stimulated by cathodal (A) stimulation and by anodal (B) for different timestamps.

When the axon is located closer or further away from the active electrode a comparison has been made between the excitation thresholds of cathodal (A) and anodal (B) stimulation as shown in Figure 6. This plot shows that for clinical DRGS values (< 1 mA [7]) the different Aβ fibers are stimulated. Another conclusion that can be made from this plot is that the values are the same for cathodal and anodal stimulation. This is due to the fact that the cathode and anode only switch. This will affect the location of first spike, but not the excitation threshold. Finally Figure 6 also shows that if the pulse width increases the excitation threshold decreases. The most significant decrease in excitation threshold can be seen if the pulse width varies from 0.1 – 0.2 ms. When increasing the pulse width any longer (0.3 – 0.5 ms) no significant decrease in activation threshold is observed, only the time of first spike will be later. This suggests that the most efficient pulse width according to the model when using a monophasic pulse is 0.3 ms.

Subsequently the effect of varying the axon diameter on the excitation threshold is studied. The diameter was varied between 5.3-11.3 µm and the result is plotted as shown in Figure 7. Note that the results for cathodal and anodal stimulation will be the same, thus only the one for cathodal stimulation is plotted.

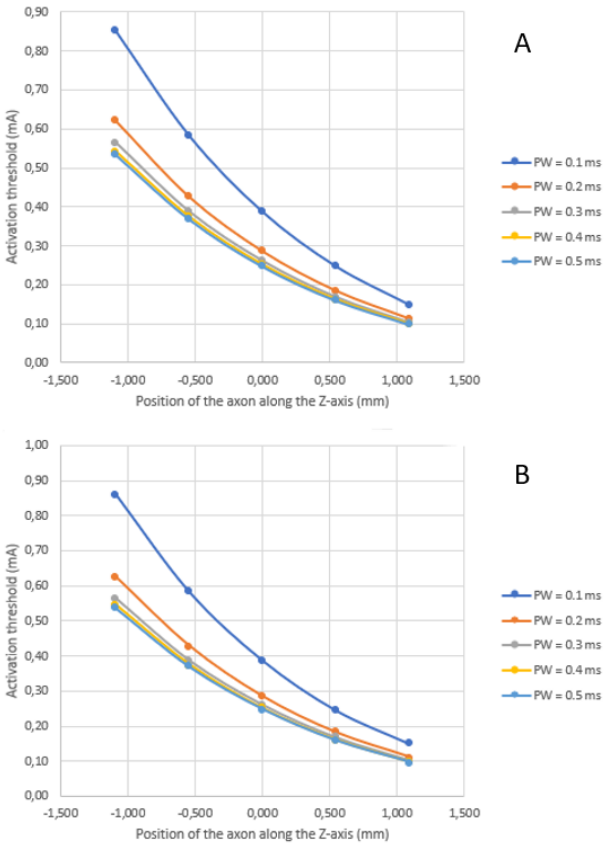

Figure 6 – Excitation threshold current versus position of the Aβ fiber along the Z-axis for cathodal (A) and anodal (B) stimulation when using different pulse widths.

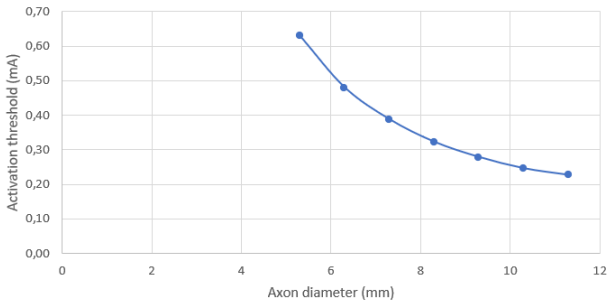

Figure 7 – Activation threshold current vs. axon diameter of the Aβ fiber located in the middle of the DRG when using a monophasic pulse with a pulse width equal to 0.1 ms.

From Figure 7 it becomes clear that when the diameter is bigger the excitation threshold will decrease. This can be explained by looking at the SENN model. The distance between the nodes of Ranvier increases proportional with the diameter. Subsequently the potential gradient between the nodes of Ranvier also increases proportional with the diameter. In addition to this the membrane capacitance, proportional with the diameter, and the axial resistance, inversely proportional with the diameter, cancel each other out. Therefore the only mechanism left to influence the relation between threshold and diameter is the distance between the nodes of Ranvier [8].

Subsequently the effect of using a biphasic versus a monophasic pulse is discussed. The case when the cathodal phase comes first followed by the anodal phase is studied and shown in Figure 8.

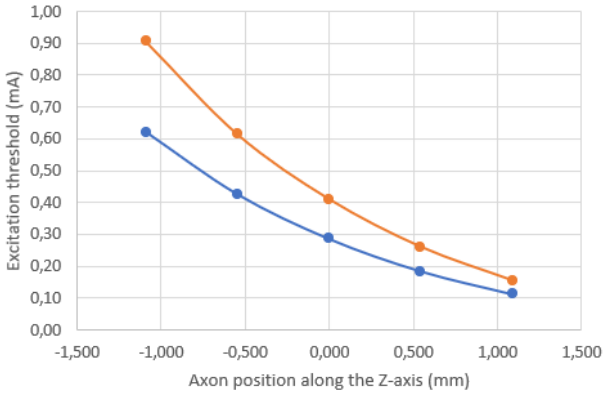

Figure 8 – Effect of using a monophasic cathodal (blue) versus a biphasic (orange) pulse with first the cathodal and second the anodal phase on the excitation threshold along different positions of the Aβ fiber along the Z-axis when using a pulse width equal to 0.1 ms.

The excitation threshold is consistently higher when using this biphasic pulse in comparison to using the monophasic pulse. This can be explained by looking back at the membrane potential plots shown in Figure 5. When first performing cathodal stimulation the depolarization will happen under the active electrode (cathode), when subsequently performing anode-like stimulation hyperpolarization will happen under the active electrode resulting a less efficient pulse. The same way of thinking can be followed for a biphasic pulse with anodal stimulation as first phase. It shown that a monophasic pulse causes tissue damage because this pulse is not charge balanced [12]. Therefore in clinical settings a biphasic pulse used.

B. Stimulation of C fibers

Not only Aβ fibers but also thin unmyelinated C fibers are studied in this thesis. In Figure 9 the excitation threshold versus the pulse width is plotted for different locations of the C fiber axon when subjected to cathodal stimulation.

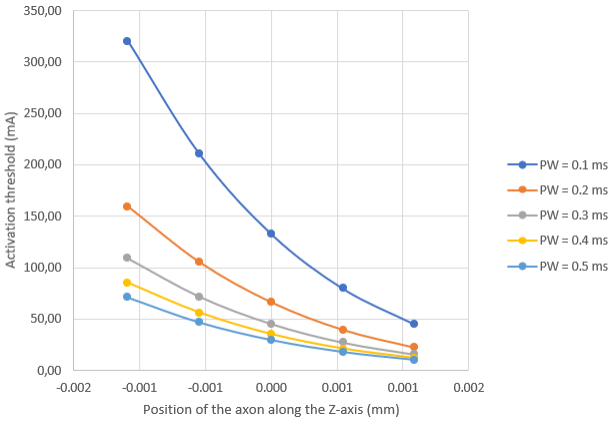

Figure 9 – Excitation threshold current versus position of the C fiber along the Z-axis for cathodal stimulation when using different pulse widths.

Because the same values occur when performing anodal stimulation, only cathodal stimulation is plotted. A first conclusion that can be drawn from this plot is that the excitation threshold decreases with increasing pulse width, similar to what

happens in Aβ fibers. Also the excitation threshold decreases if the axon is positioned further away from the active electrode. This is logical because the electric field emitted by the electrode is weaker further away from the electrode. Finally it can be seen that these excitation thresholds vary from 320.23 – 10.01 mA which are values far outside clinical ranges.

C. *Stimulating a nerve fiber bundle*

To determine the influence of the distance from the center of the electrode shaft to the center of the DRG a nerve fiber bundle consisting of 19 Aβ fibers is stimulated by cathodal stimulation. The percentage of activated neurons by stimulation amplitudes between the clinical range of 1 mA is plotted versus the center to center distance between the electrode shaft and the DRG as shown in Figure 10. This plot shows that a high amount of nerve fibers is activated when the center to center distance is within 3.65 – 6.75 mm. From this point on the curve shows a steep fall. This suggests that the electrode shaft should be implanted within the range of 3.65 – 6.75 mm center to center distance between the active electrode and the DRG.

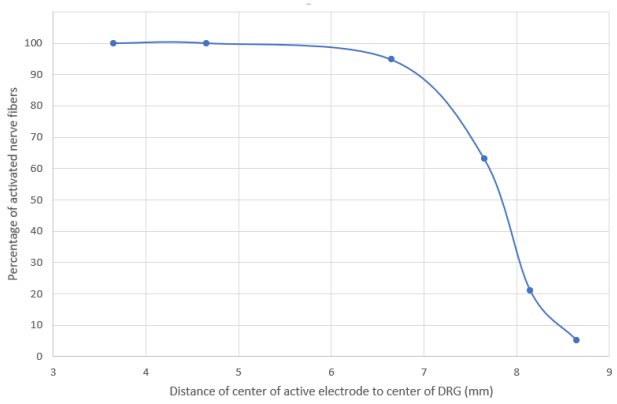

Figure 10 – Percentage of activated Aβ nerve fibers versus the center to center distance between the active electrode and the DRG when performing cathodal stimulation.

IV. Limitations and Future Work

It is important that the limitations of this model are well understood to correctly interpret the results presented in this work. Also future studies are necessary to further optimize the promising DRGS technique.

The DRG actually consists of pseudo-unipolar neurons that consist of a soma and a T-junction bifurcating into a distal and proximal process. To create this bifurcation is not possible in Sim4Life, hence in this model a more simplistic straight line axons are used.

The model created in this thesis is a cylindrical model. These ideal cylinders do not resemble the actual shape of the DRG which is much more complex.

Two types of neuron fibers are studied in this master dissertation which are Aβ and C fibers. Actually more fiber types should be studied to better understand the technique. Especially Aδ fibers are of interest. These fibers are also myelinated but not as much as the thick myelinated Aβ fibers. They play a major role in conducting mechanical and thermal pain [11]. Consequently it is important to study the involvement and the behavior of these Aδ fibers when performing DRGS.

In this master dissertation one type of electrodes is studied namely cylindrical electrodes on a straight electrode shaft. In further studies it could be feasible to study multiple types of electrodes.

V. Conclusion

In this master dissertation a model of the DRG is constructed in the software Sim4Life to study the behavior of Aβ and C fibers when exposed to DRGS. These nerve fibers were modelled by using respectively the SENN and Sundt model. Subsequently anodal and cathodal stimulation is performed to study how these fibers react to different types of DRGS. Thereafter an analysis is made in which the effect of parameters on these nerve fibers such as varying axon position, axon diameter, pulse width and pulse type is assessed. Subsequently a nerve fiber bundle is stimulated to determine the influence of the distance between the electrodes and the DRG. After generating the results a discussion is made in which these results are explained.

The results showed that C fibers are not directly stimulated by DRGS when using clinical values for the applied current according to this model. When studying Aβ fibers it was suggested that the most efficient way of stimulation was a monophasic pulse with a pulse width of 0.3 ms, but because a monophasic pulse causes tissue damage a biphasic pulse is used in clinical settings. Finally the model showed that the electrode shaft should be implanted within the range of 3.65 – 6.75 mm center to center distance between the active electrode and the DRG.

VI. References

[1] Esposito, Malayil, M. F, Hanes, Rudy, Deer and Timothy, “Unique characteristics of the dorsal root ganglion as a target for neuromodulation,” *Pain Medicine*, pp. S23-S30, 2019.

[2] Pope, J. E, Deer, T. R, Kramer and J. , "A Systematic Review: Current and Future Directions of Dorsal Root Ganglion Therapeutics to Treat Chronic Pain," *Pain medicine*, vol. 14, no. 10, pp. 1477-1496, 2013.

[3] Breivik, Harald, Collett, Beverly, Ventafridda, Vittorio, Cohen, Rob and Gallacher, "Survey of chronic pain in Europe: prevalence, impact on daily life, and treatment," *European journal of pain*, vol. 10, no. 4, pp. 287-333, 2006.

[4] Kumar, Krishna, Rizvi, Syed, Bnurs and S. Bishop, "Spinal cord stimulation is effective in management of complex regional pain syndrome I: fact or fiction," *Neurosurgery*, vol. 69, no. 3, pp. 566-580, 2011.

[5] J. Holsheimer, "Which neuronal elements are activated directly by spinal cord stimulation," *Neuromodulation: Technology at the Neural Interface*, vol. 5, no. 1, pp. 25-31, 2002.

[6] Lempka, Scott, Patil and Parag, "Innovations in spinal cord stimulation for pain," *Current opinion in biomedical engineering*, vol. 8, no. 1, pp. 51-60, 2018.

[7] R. D. Graham, T. M. Burnes, B. Duan and Lempka, "Dorsal root ganglion stimulation for chronic pain modulates Aβ-fiber activity but not C-fiber activity: A computational modeling study," *Clinical Neurophysiology*, vol. 130, no. 6, pp. 941-951, 2019.

[8] Reilly, Freeman, Larkin and Willard, "Sensory effects of transient electrical stimulation-evaluation with a neuroelectric model," *IEEE transactions on biomedical engineering*, no. 12, pp. 1001-1011, 1985.

[9] McNeal, "Analysis of a Model for Excitation of Myelinated Nerve," *IEEE Transactions on Biomedical Engineering*, Vols. BME-23, no. 4, pp. 329-337, 1976.

[10] D. Sundt, N. Gamper and D. Jaffe, "Spike propagation through the dorsal root ganglia in an unmyelinated sensory neuron: a modeling study," *Journal of neurophysiology*, vol. 114, no. 6, pp. 3140-3153, 2015.

[11] Hu, Cai and Xiao, "Human brain responses to concomitant stimulation of Aδ and C nociceptors," *Journal of Neuroscience*, vol. 34, no. 34, pp. 11439-11451, 2014.

[12] S. F. Cogan, S. Hara and K. A. Ludwig, "Chapter 7 - The Safe Delivery of Electrical Currents and Neuromodulation," in *Neuormodulation - Comprehensive Textbook of Principles, Technologies, and Therapies*, Academic press, 2018, pp. 83-94.

Contents

List of Figures

List of Tables

List of abbreviations

AP	Action potential
CNS	Central nervous system
CSF	cerebrospinal fluid
DBS	Deep brain stimulation
DRG	Dorsal root ganglion
DRGS	Dorsal root ganglion stimulation
IASP	International Association for the Study of Pain
KDR	K^+ delayed-rectifier channels
Na_v	Voltage-gated Na^+ channel
PNS	Peripheral nervous system
PSNS	Parasympathetic nervous system
SCS	Spinal cord stimulation
SENN	Spatially Extended Nonlinear Node
SNS	Sympathetic nervous system

List of symbols

ϕ	Electrode voltage
ρ_{i}	Resistivity of the axoplasm
$\mathbf{a(t)}$	Modulating pulse
$\mathbf{c}_{\mathrm{m}}$	Membrane capacitance per unit area
$\mathbf{C}_{\mathrm{m}}$	Membrane capacitance
$\mathbf{d}$	axon diameter
$\mathbf{D}$	Fiber diameter including myelin
$\mathbf{E}_{\mathrm{r}}$	Potential source to maintain the resting potential
$\mathbf{g}_{\mathrm{m}}$	Subthreshold membrane conductance per unit area
$\mathbf{G}_{\mathrm{a}}$	Internodal conductance
$\mathbf{G}_{\mathrm{m}}$	Membrane conductance
$\mathbf{I}_{\mathrm{i}}$	Ionic current
$\mathbf{J}$	current density
$\mathbf{L}_{\mathrm{i}}$	Internodal length
$\vec{n}$	Normal vector
$\mathbf{r}$	distance to electrode
$\mathbf{R}_{\mathrm{a}}$	Resistance of the axoplasmic fluid
$\mathbf{R}_{\mathrm{m}}$	Membrane resistance
$\mathbf{S}$	Surface
$\mathbf{T}$	Titration factor
$\vec{v}$	Vector field
$\mathbf{V}_{\mathrm{n}}$	Membrane potential at the n^{th} node
$\mathbf{w}$	nodal gap

Chapter 1

Introduction

This section contains an introduction to the master dissertation 'computational modelling of dorsal root ganglion stimulation for pain relief'. In this introduction the human nervous system and its subdivisions are described followed by an explanation of the term "pain" and the role of different nerve fiber types in the study of pain. Subsequently the anatomy and functions of the dorsal root ganglion are discussed as well as the term chronic pain and the current treatment options. Finally a description of the thesis objective is given.

1.1 The human nervous system

The human nervous system can be divided into two main sections: the peripheral and the central nervous system (Mai & Paxinos, 2011) as shown in Figure 1.1.

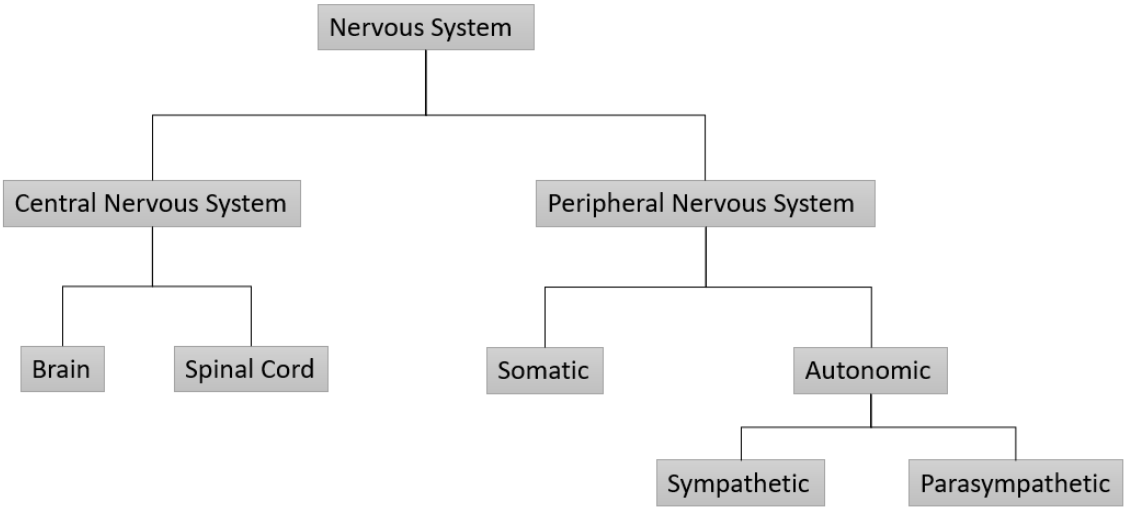

Figure 1.1: Division of the human nervous system adapted from Mai et al. (2011).

The peripheral nervous system (PNS) can be further subdivided into the somatic and the autonomic nervous system. The somatic nervous system is responsible for voluntary control of body movements (Akinrodoye & Lui, 2020). It consists of sensory and motor neurons in the skin, joints and muscles. The autonomic nervous system regulates involuntary events (e.g. respiration, digestion, etc) (McCorry, 2007). The autonomic nervous system can further be divided into the sympathetic (SNS) and the parasympathetic nervous system (PSNS). The SNS can accelerate heart rate and inhibit digestion while the PSNS does the opposite. The SNS is also associated with the fight-or-flight reaction of the body in which it ensures that the adrenal glands release hormones such as adrenaline and cortisol (McCorry, 2007).

The central nervous system (CNS) consists of the brain and the spinal cord (Brodal, 2004). Two major components of the brain are white and gray matter. White matter contains myelinated axons while gray matter has unmyelinated cell bodies and dendrites. The spinal cord begins at the level of the brainstem and is responsible for sensory and motor innervation of almost all structures below the neck. The white matter is located outside the spinal cord while the gray matter is located inside. Information is typically collected from the periphery and send to the dorsal side of the spinal cord through dorsal nerves. The cell bodies of these sensory neurons are located in the dorsal root ganglion (DRG) (Brodal, 2004).

1.2 Pain

The definition of pain according to the International Association for the Study of Pain (IASP) is: "An unpleasant sensory and emotional experience associated with, or resembling that is associated with, actual or potential tissue damage" (IASP, 2020). Furthermore is chronic pain defined as continuous pain that lasts for at least 12 weeks (healthline, 2017). From these definitions it becomes clear that pain is subjective rather than objective. This makes pain one of the hardest fields to study which poses a significant challenge to scientists studying this issue.

The importance of researching pain and pain relief treatments can be stressed by the following facts. Studies show that 20.4% of US adults suffer from chronic pain (Zelaya, Dahlhamer, Lucas, & Connor, 2020). This does not only consist of physical pain, but also emotional pain (anxiety, depression, isolation, ...) as stated in the definition. Both these factors can have severe consequences like limited life and/or work activities.

The nervous system is responsible for experiencing pain. This nervous system consists of nerve fibers which are classified according to fiber diameter and conduction velocity (Erlanger & Gasser, 1937). The classification system was introduced by Erlanger and Gasser and later adapted by Terzis and Smith (Terzis & Smith, 1990). A-fibers are largely myelinated, B-fibers are less myelinated and C-fibers are unmyelinated. Somatic efferent and afferent nerve fibers are part of group A and are subdivided according to decreasing size (Aα, Aβ, Aγ and Aδ). B-fibers are exclusively visceral nerve fibers (e.g. vagus nervus). Finally group C includes autonomic postganglionic fibers and somatic afferent nerve fibers. The different types of fibers and their characteristics can be seen in Table 1.1.

Table 1.1: Nerve fiber classification (Terzis et al., 1990)

Fiber Type	Subtype	Functions		Diameter (μm)	Conductance Velocity (m/s)	Spike Duration (ms)	Absolute Refractory Period (ms)
A	α	Myelinated somatic	Proprioception, somatomotor	12-20	70-120	0.4-0.5	0.4-1
	β	afferent and efferent	Touch, pressure	5-12	30-70		
	γ		Motor for muscle spindles	3-6	15-30		
	δ		Pain, cold, touch	2-5	12-30		
B		Myelinated pregnanglionic autonomic		<3	3-15	1.2	1.2
C	Dorsal horns	Unmyelinated somatic afferent	Pain, temperature mechanoreception, reflex response	0.5-2	0.5-2	2	2
	Sympathetic	Unmyelinated autonomic postganglionic	Pilomotor, sudomotor and vasomotor	0.7-2.3	0.7-2.3	2	2

1.2.1 The role of Aβ fibers in studying pain

Aβ fibers are heavily myelinated fibers with a relatively large diameter. In the skin, for example, they are responsible for touch. Aβ fibers are also present in the dorsal root ganglion (Berta, Qadri, Tan, & Ji, 2017).

Nociceptors (pain receptors) have high thresholds for activation. Subsequently they can only be activated by intense stimuli such as damaging stimuli or stimuli that can potentially damage tissue. It is proven in literature that a significant amount of A fiber nociceptors conduct in the Aβ conduction velocity range (Djouhri & Lawson,

2004). Conduction velocities of up to 75 m/s are recorded in mammals (Burgess & Perl, 1967). This means that there are A fiber nociceptive units with conduction velocities in the Aβ range. Thus it is important to study these fibres.

1.2.2 The role of C fibers in studying pain

C fibers are thin unmyelinated fibers with a low conduction velocity which respond to intense stimuli. Theory believes that mainly the slow conduction velocity of the C fibers is responsible for the so-called "second pain" (Berta et al., 2017). This second pain can often be widespread and long lasting. C fibers can react to different types of stimuli: chemical, mechanical or thermal and are therefore categorized as polymodal.

In this thesis both these types of fibers will be studied as they both play a major role in the study of pain.

1.3 The dorsal root ganglion

The DRG is responsible for the transmission of sensory signals from receptors such as thermoreceptors, nociceptors, proprioceptors and chemoreceptors to the CNS. In this subsection the anatomy and function of the DRG will be introduced.

1.3.1 Anatomy of the DRG

The DRG, shown in Figure 1.2, is a bilateral structure located within neuroforamen (bony vertebral structures) which exists at every section of the spine (Esposito, Malayil, Hanes, & Deer, 2019). The DRG is an extension of the dorsal root in which approximately 15 000 neurons are present. These neurons form neuron bundles (nerves) which contain a variation of nerve fibers including: C fibers, high-threshold Aβ nociceptors and finally Aδ fibers (Esposito et al., 2019). The fibers that will be studied in this thesis are the Aβ and C fibers which are described in subsection 1.2. The somata of the DRG are separated by satellite glial cells (SGC) which inhibit the interaction between cell bodies (Znaor, Lovrić, Hogan, & Sapunar, 2007).

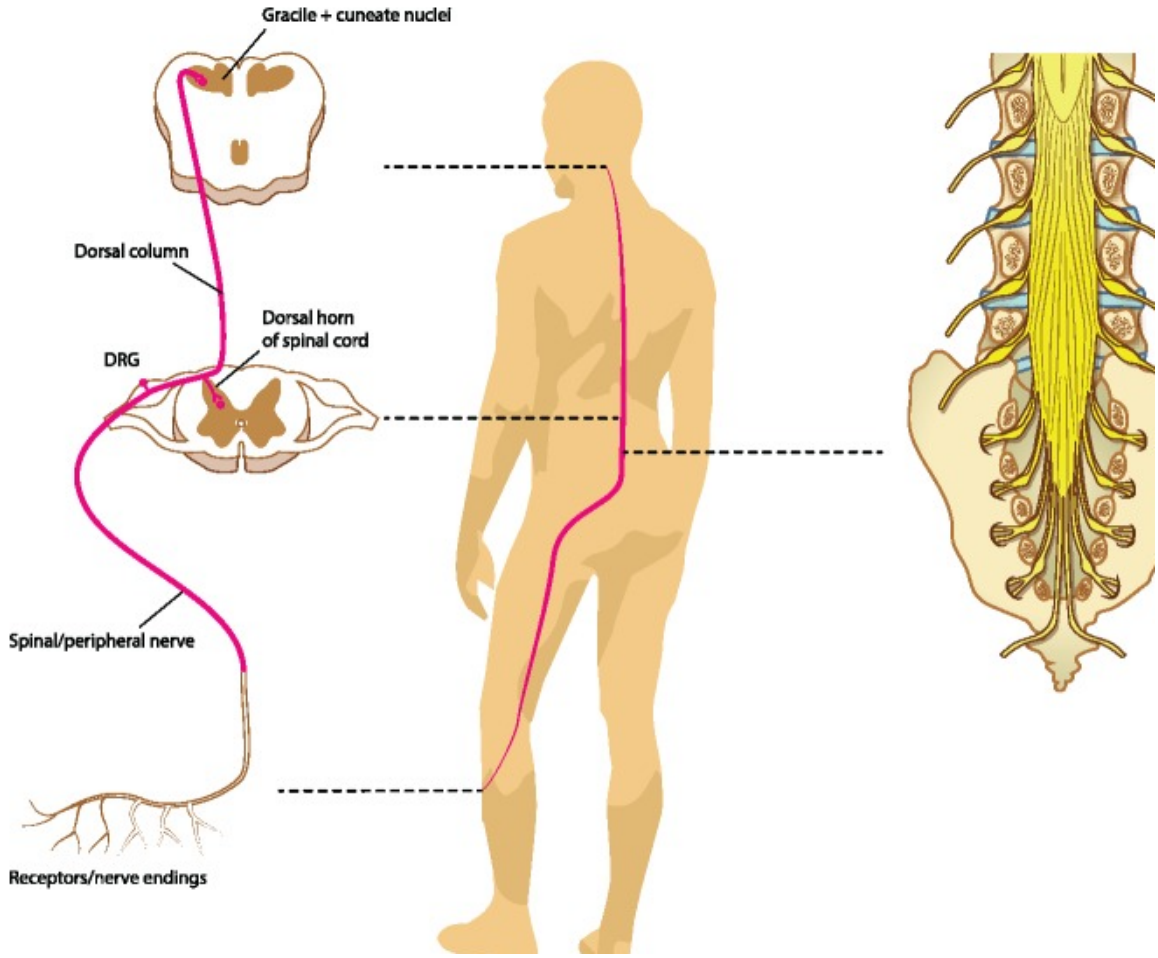

Figure 1.2: Expansion of a primary sensory neuron, position of the dorsal root ganglion and cross-section of the spinal cord (Left). Position of the dorsal root ganlia inside the lumbar and sacral spine (Right) (Esposito et al., 2019).

DRG neurons are pseudo-unipolar. These types of neurons consist of an axon that bifurcates into two branches. One of them travels to the PNS while the other travels to the CNS as shown in Figure 1.2 (Leijnse & D'Herde, 2016). The axon that extends to the CNS terminates in synapses at ipsilateral or contralateral wide dynamic range neurons, inhibitory interneuron networks and other targets in the dorsal horn (Esposito et al., 2019). Other nerve fibers from the DRG extend to the dorsal column and further on to the brainstem. These fibers are typically Aβ fibers which are largely myelinated. These are also the fibers that are mostly stimulated in spinal cord stimulation (Oakley & Prager, 2002).

The locations of the dorsal root ganglia inside the lumbar and sacral spine are visible on the right side of Figure 1.2. Majoritively two kinds of studies are used to detect these locations: Magnetic resonance imaging (MRI) studies and research on cadavers.

MRI research in healthy subjects showed that most of the L1-L4 dorsal root ganglia (97.8-100%) are present in the foramen. This is slightly less at L5 with 94.3% and a small percentage laying in the intraspinal region (5.7%) (Shen, Wang, Chen, & Liang, 2006).

1.3.2 Function of the DRG

The main function of the DRG is the transmission of sensory messages from thermoreceptors, nociceptors, proprioceptors and chemoreceptors to the CNS (Pope, Deer, & Kramer, 2013). The DRG also has a unique feature, the action potentials (APs) generated by impulses of the periphery can also bypass the DRG and travel to the proximal process or the spinal cord. This is due to the embryological onset as a bipolar neuron before evolving into the pseudo-unipolar form (Ahimsadasan & Kumar, 2018).

1.3.3 Chronic pain and treatment options

Chronic pain is defined as persistent pain that lasts longer than 12 weeks despite medication or treatment (Andersson, 1999). Normally pain settles down with time but in some cases the brain doesn't stop sending out pain signals. The source of this phenomenon isn't always clear, thus it can be very hard to find a suitable treatment. Chronic pain doesn't consist of the visible physical pain alone, but also comes with mental health issues such as depression and anxiety as mentioned in Section 1.2.

Drug related treatments are one of the most used treatments for chronic pain (e.g. pain killers). Non-drug treatments consist of exercise, heat and/or cold application, massage, spinal cord stimulation (SCS), dorsal root ganglion stimulation (DRGS) and deep brain stimulation (DBS) (Breivik, Collett, Ventafridda, Cohen, & Gallacher, 2006).

1.3.4 Drug treatments

One of the most used treatments for chronic pain is drugs such as analgesics (pain relievers). Well known non-narcotic analgesics are ibuprofen, aspirin and naproxen.

Also opioid analgesics are used in some cases. These opioid analgesics are associated with poor physical health, poor mental health, activity limitations, addiction and physical inactivity (Toblin, Mack, Perveen, & Paulozzi, 2011). Again, this emphasizes the fact that other treatments such as DRGS need to be investigated. Opioid drugs are also associated with overdose deaths especially in patients who are diagnosed with

mental ilness (Toblin, Paulozzi, Logan, Hall, & Kaplan, 2010). These opioid drugs are in general prescribed to patients with more severe pain. A study showed that 80-90% of opioid users experience moderate to severe pain and their mean pain severity score is higher than patients who are not using opioid drugs (Eriksen, Sjøgren, Bruera, Ekholm, & Rasmussen, 2006).

Other drugs for pain relief are topical products (e.g. Lidocaine creams or patches), antidepressants (e.g. Alprazolam and Lorazepam), anticonvulsants (anti-epileptics), sedatives, muscle relaxants, corticosteroids, antirheumatics, etc.

1.3.5 Spinal cord stimulation

Spinal cord stimulation is built on the principle of the gate theory. This theory states that there is a gate in the dorsal horn on the spinal cord that controls the transmission of pain (Melzack & Wall, 1996). According to Melzack et al. the gate opens when a large amount of small over large afferent nerve fiber activity exists in the peripheral nerve system. Subsequently the gate closes when a large amount of large-diameter afferent nerve activity exists. Based on this theory medicine focused on closing this gate by selectively stimulating the large-diameter afferent fibers. This could result in the reduction of pain input. Unfortunately some issues arise when further investigating this theory. E.g. empirical data shows that instead of both acute and chronic pain being reduced, SCS only reduces chronic pain (Oakley & Prager, 2002). The real mechanism is thus much more complex.

In principle SCS works by applying current to electrodes, this current spreads onto the dorsal dura and activates nerve fibers in the dorsal columns with two kinds of impulse transmission: orthodromic (1) and antidromic (2) (Linderoth & Foreman, 1999). After SCS, patients experience paraesthesias instead of the pain they felt initially. This is caused by the orthodromic impulses. The antidromic impulses are responisble for excitation in the outer laminae by activating the gate-mechanism (3). This mechanism has an inhibitory influence on the transmission in the small diameter fibers, thus reducing pain. The principle is elaborated by means of Figure 1.3.

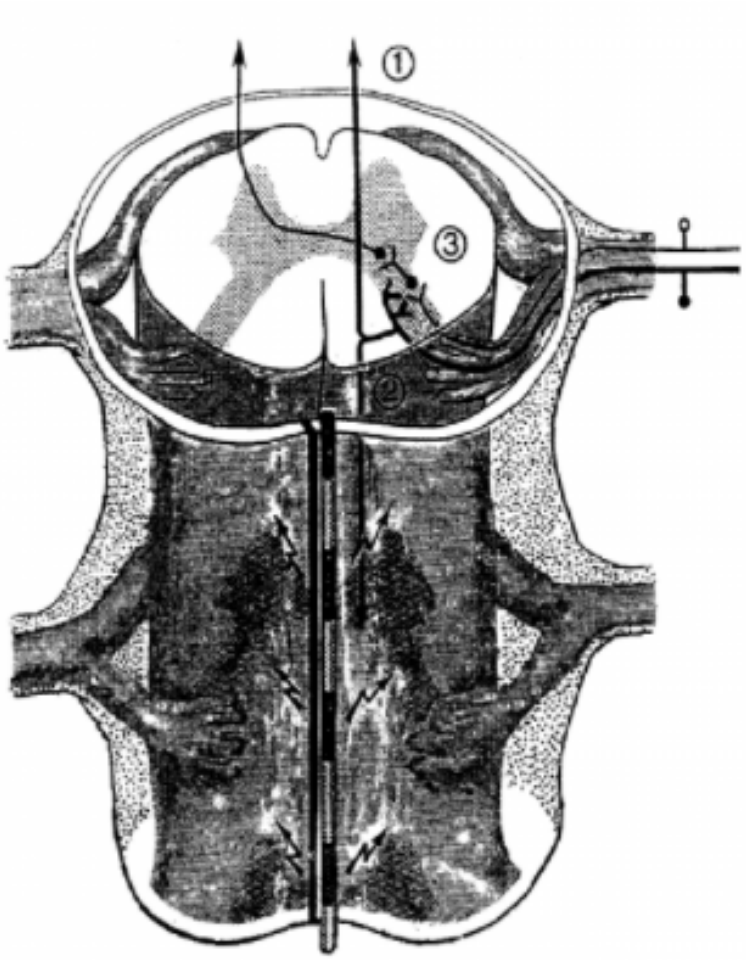

Figure 1.3: Working principle of spinal cord stimulation: (1) orthodromic, (2) antidromic, (3) gate-mechanism (Linderoth et al., 1999).

1.3.6 Dorsal root ganglion stimulation

In spite of the fact that SCS shows good clinical results, as described in section 1.4.2, several limitations to the technique exist. Due to the anatomy of the spinal cord certain regions are difficult to reach by conventional SCS (e.g. bladder, feet) (Kumar, Rizvi, & Bnurs, 2011). In addition to this, a high amount of cerebrospinal fluid (CSF) is present around the spinal cord. This CSF is highly conductive which results in the occasional shunting of the electrical current, away from the target regions (Holsheimer, 2002). Another limitation is that the leads in SCS are susceptible to positional changes over time. For example, These lead migrations can happen when the patient experiences postural changes when aging. The changes in position of the leads relative to the spinal cord result in a less accurate delivery of the electrical current to the target regions (Lempka & Patil, 2018).

In DRGS a cylindrical electrode is implanted in the intraforaminal epidural space above the DRG (Graham, Bruns, Duan, & Lempka, 2019). Due to the fact that the intraforaminal space is compact and the absence of large amounts of CSF around the DRG (Brierley, 1950), the leads used in DRGS remain close to the DRG and are less prone to positional changes in contrast to SCS. Due to the fact that a DRG innervates one single dermatome, DRGS could ensure dermatome-specific pain relief. This means that regions that were hard to reach using SCS (e.g. bladder) could now be reached by using DRGS. The modulation pulse is applied by using an implantable pulse generator (IPG). This IPG is typically implanted in the posterior lateral flank below the Scarpa's fascia (Deer et al., 2019). To minimize any stress on the leads crossing over the spine, the IPG is implanted on the same side as the lead entry on the contralateral side of the DRG that is targeted (Deer et al., 2019). In addition strain-relief loops can be inserted in the IPG pocket to reduce further stress and traction on the leads.

In spite of the fact that the mechanism of action of DRGS is not yet fully understood, electrical stimulation of the DRG is proven to work and shows a relatively high success rate of adequate pain relief in 75% of patients in preliminary clinical studies (Deer et al., 2017).

When considering these limitations and the role of the DRG in managing pain, it becomes clear that DRGS could bring a solution or a better solution for patients experiencing focal chronic pain. However partly due to the complexity and partly due to the novelty, this technique is far from optimized.

Future directions that are being explored right now are: full MRI compatibility, DRG paddle leads and hybdrid systems (Deer et al., 2019). Full MRI compatibility would mean that the need for explant would be less, this is approved with certain devices with 50 cm leads, but not for 90 cm leads. By using DRG paddle leads difficult accessible spinal segments could be reached, clinical studies should be done soon. Finally hybdrid systems could ensure that SCS and DRGS leads could be connected to the same IPG, which would reduce the need for surgery and the amount of implanted devices.

1.4 Thesis objective

The objective of this master dissertation is first to create a model of the DRG and surrounding structures including an electrode shaft responsible for the electrical stimulation. Subsequently this model has to be coupled with neuronal models to study the behaviour of Aβ and C fibers to further optimize the DRGS technique. Optimization includes influence of the modulating pulse type and length, anodal versus cathodal stimulation, influence of varying axon fiber diameters and influence of varying positions of the different nerve fibers within the DRG. After generating the results of varying these parameters, a thorough analysis has to be performed and comparisons between the different results have to be made.

.

Chapter 2

Methods

In this section the methods used to generate the results are explained. First of all the electromagnetic and neuronal models that are used are described. Subsequently the methods for determining the activating function and excitation thresholds are explained. After this more information about the modulating pulse is given and finally the written Python and Matlab scripts and their functions are explained.

2.1 Model of the DRG

The computational model for electrical stimulation of the DRG is made in the software Sim4Life (version 5.2.1.1375). This software provides a programming environment that allows the users to create an anatomical model, to simulate data with the model and to analyze the generated data. The thesis starts off with developing a model of the DRG.

The anatomical model of the DRG is based on the model created in "Dorsal root ganglion stimulation for chronic pain modulates Ab-fiber activity but not C-fiber activity: A computational modeling study" (Graham et al., 2019).

The anatomy of the finite element model of a human L5 DRG is illustrated in Figure 2.1.

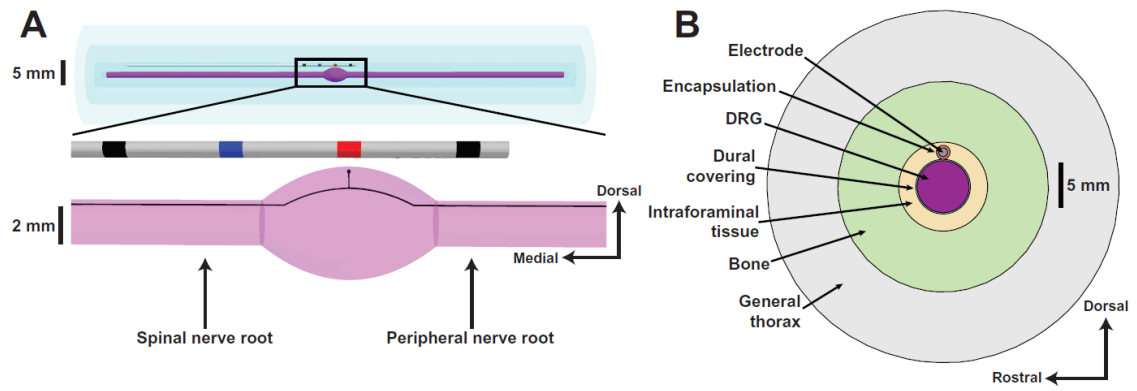

Figure 2.1: The anatomy of the finite element model of a human L5 DRG. (A) Side view of the DRG. The electrode shaft is included (red: active electrode, blue: return electrode, black: inactive electrode) (B) Cross section of the DRG (Graham et al., 2019)

The side view of the DRG and electrode shaft is shown in Figure 2.1 (A). The active electrode is placed right above the DRG. The black line is an example primary sensory neuron trajectory. The cross section through the middle of the DRG is shown on the right side of Figure 2.1 (B). The model consists of the DRG surrounded by dural covering, intraforaminal tissue, bone and general thorax. The encapsulation of the electrodes is also included. The model constructed in this thesis is based on the one described in this paragraph and can be seen in Figure 2.2 with in the left bottom corner the coordinate system. The colors of the X-, Y- and Z-axis are respectively red, green and blue.

The model is created in such fashion that the middle of the DRG is located at position (0, 0, 0). This is mentioned to correctly interpret and fully understand the results later in this master dissertation.

The anatomical parameters can be seen in Table 2.1 and the electrical conductivity of each component is shown in Table 2.2.

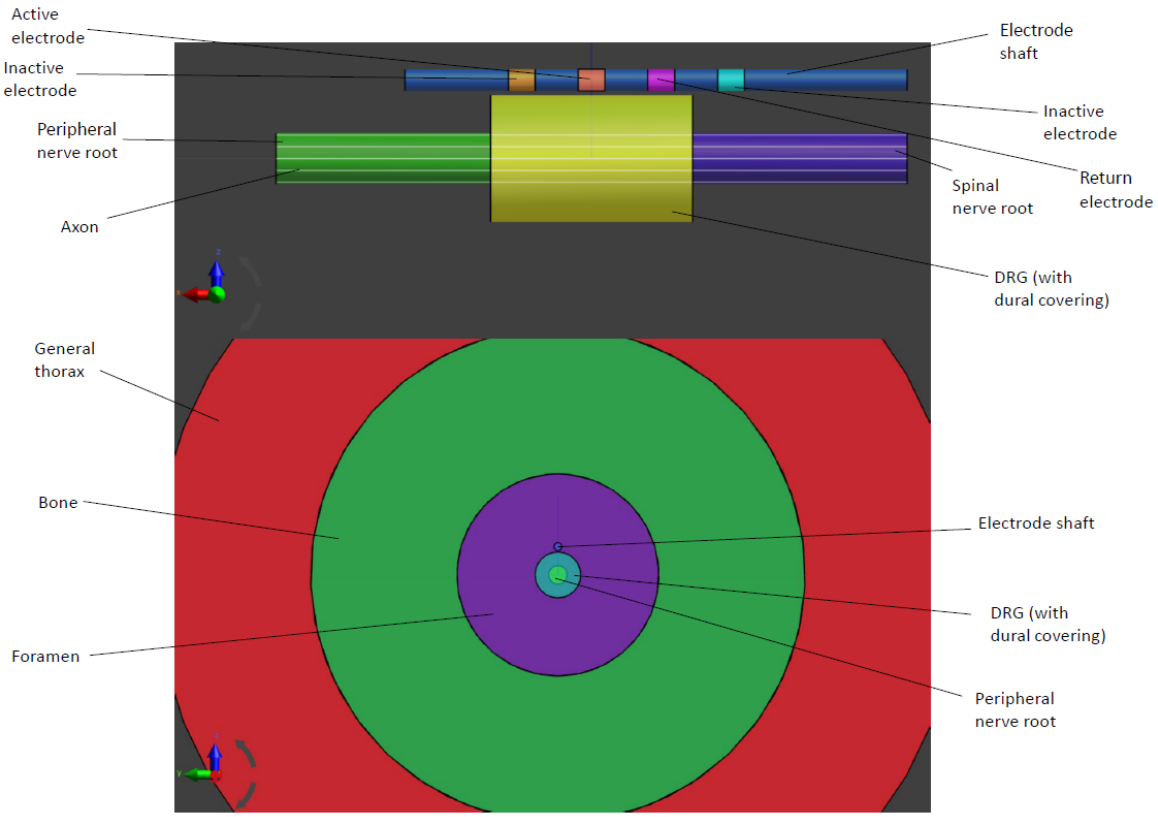

Figure 2.2: The constructed model used in this thesis of a human L5 DRG with annotation of all elements.

Table 2.1: Anatomical parameters for the human L5 DRG model (Graham et al., 2019)

Parameter	Value	Reference
DRG length	9,4 mm	(Hasegawa et al., 1996)
DRG width	5,9 mm	(Hasegawa et al., 1996)
Nerve root radius	1,19 mm	(Hogan, 1996)
Dural sheath thickness	150 μm	(Reina et al., 2007)
Foramen height	10,1 mm	(Silverstein et al., 2015)
Encapsulation layer	0,3 mm	(Grill and Mortimer), 1994)
Electrode contact length	1,25 mm	(Amirdelfan et al. 2018)
Electrode radius	0,5 mm	(Amirdelfan et al. 2018)

Table 2.2: Electrical conductivity parameters for the human L5 DRG model (Graham et al., 2019)

Parameter	Value	Reference
Gray matter	0,23 S/m	(Geddes and Baker, 1967)
White matter	0,6 S/m	(Geddes and Baker, 1967)
Dural covering	0,6 S/m	(Lempka et al., 2015)
General tissue	0,25 S/m	(Geddes and Baker, 1967)
Bone	0,02 S/m	(Gabriel et al., 1996)
Encapsulation	0,17 S/m	Grill and Mortimer, 1994)
Electrode contact length	1,25 mm	(Amirdelfan et al. 2018)
Electrode radius	0,5 mm	(Amirdelfan et al. 2018)

2.2 Modelling Aβ fibers

The SENN model (Spatially Extended Nonlinear Node) is used to simulate the behavior of Aβ fibers. Aβ fibers are largely myelinated in contrast to the small non-myelinated C fibers (Devor, 1999, 2009; Djouhri et al., 2006). The general concept of a myelinated fiber subjected to an induced electrical field is shown in Figure 2.3.

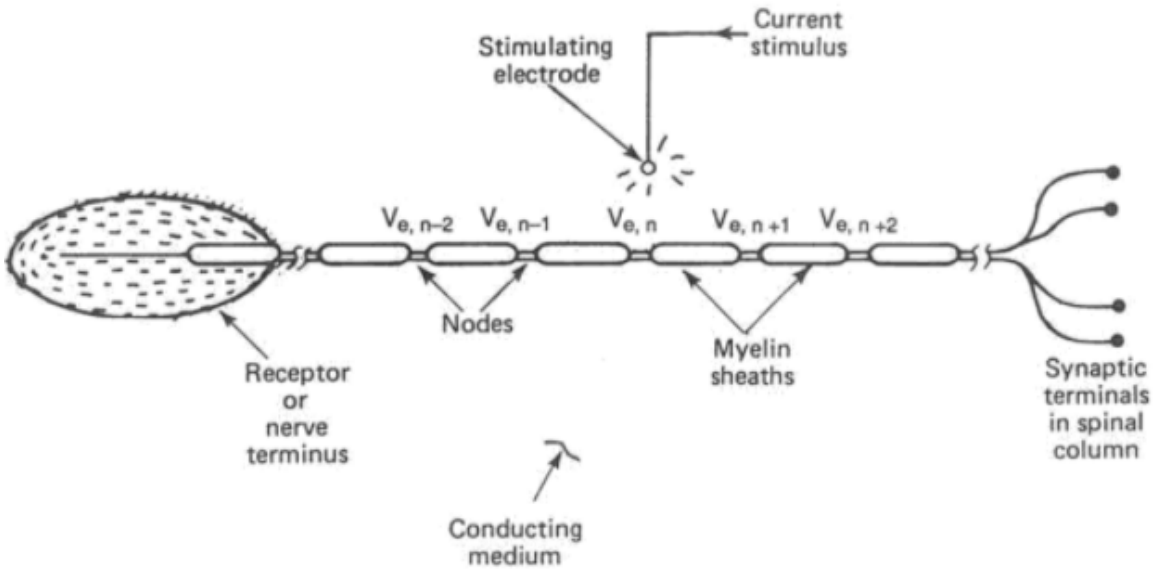

Figure 2.3: General concept of a myelinated fiber subjected to an induced electrical field (McNeal et al., 1976).

A stimulus current is used to induce an electrical field originating in the stimulating electrode. This current subsequently travels through the conducting medium and

reaches the myelinated fiber. This current then causes voltage disturbances $V_{e,n}$ at the nodes of the fiber. These disturbances will cause de- or hyperpolarization of the membrane, depending on the direction of the current (Reilly & Diamant, 2011).

2.2.1 SENN model

The equivalent electrical circuit of a myelinated fiber is illustrated in Figure 2.4.

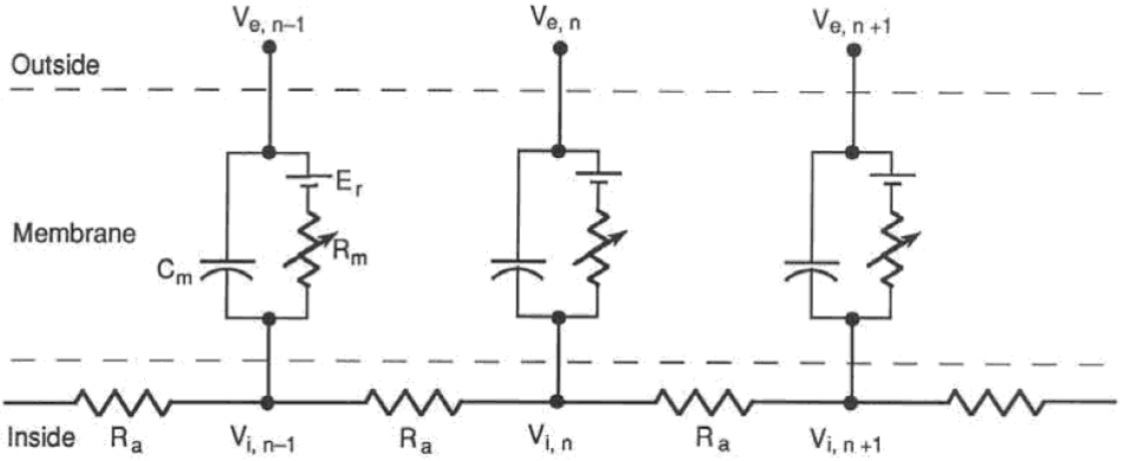

Figure 2.4: The equivalent electrical circuit of a myelinated fiber (McNeal et al., 1976).

The nodes are represented as a circuit consisting of a capacitance C_m, resistance R_m and a potential source E_r. This source is implemented into the circuit to maintain the resting potential of the membrane. This resting potential results from the differences in ionic concentration between the inside and the outside of the neuron and the different conductance values of the ion species. These circuits are connected through the resistance R_a which represents the resistance of the axoplasmic fluid. Each ionic species has a different conductance in the SENN model, unlike in Figure 2.4. The myelin internodes are modelled as perfect insulators. This model has potential to be expanded to include passive myelin properties, but this will increase the complexity drastically. Reilly et al. (1985) have consciously chosen to not include these passive myelin properties. This is not necessary because of the high resistance and the low capacitance of myelin. In conclusion is the SENN model a compromise between a simple single-node model and a node-plus-myelin model.

The current in the n^{th} node is equal to the sum of both capacitive and ionic currents as shown in equation 2.1:

$$C_m \frac{dV_n}{dt} + I_{i,n} = G_a(V_{i,n-1} - 2V_{i,n} + V_{i,n+1}) \tag{2.1}$$

C_m represents the membrane capacitance of the node, G_a is the inverse of R_a and represents the internodal conductance. $V_n = V_{i,n}$-$V_{e,n}$ is the transmembrane potential at the n^{th} node. The ionic current flowing across the n^{th} node is represented by $I_{i,n}$ and $V_{i,n}$ is the interior voltage at the n^{th} node. The transmembrane potential V_n is implemented as relative to the resting potential. Subsequently when V_n is negative hyperpolarization will occur and when V_n is positive depolarization will take place. More important relationships of the SENN model are given by following equations:

$$G_a = \frac{\pi d^2}{4\rho_i L_i} \tag{2.2}$$

$$G_m = g_m \pi d w \tag{2.3}$$

$$C_m = c_m \pi d w \tag{2.4}$$

In equation 2.2 d is the diameter of the axon at the node, ρ_i is the resistivity of the axoplasm and L_i is the internodal length. Subsequently is G_m in equation 2.3 the inverse of R_m which represents the membrane conductance at a node, g_m is the subthreshold membrane conductance per unit area and w is the nodal gap. Finally in equation 2.4, c_m is the membrane capacitance per unit area.

The internodal distance L_i in equation 2.2 depends on the fiber diameter D and their relation is given by equation 2.5:

$$L_i = 100D \tag{2.5}$$

D is the fiber diameter including the myelin and $d = 0.7D$ is the diameter at the node.

As mentioned before the transmembrane potential V_n is given by the equation below:

$$V_n = V_{i,n} - V_{e,n} \tag{2.6}$$

Equation 2.6 can be used to derive a differential equation for V_n (discrete form of the cable equation) by substituting 2.6 into 2.1 and rearranging the terms. The result is shown in equation 2.7.

$$\frac{dV_n}{dt} = \frac{1}{C_m}[G_a(V_{n-1} - 2V_n + V_{n+1} + V_{e,n-1} - 2V_{e,n} + V_{e,n+1}) - I_{i,n}] \tag{2.7}$$

The term $I_{\mathrm{i,n}}$ becomes linear when below threshold and nonlinear near threshold value.

$$I_{\mathrm{i,n}} = G_{\mathrm{m}} V_{\mathrm{n}} \tag{2.8}$$

$$I_{\mathrm{i,n}} = \pi dw(J_{\mathrm{Na}} + J_{\mathrm{K}} + J_{\mathrm{L}} + J_{\mathrm{p}}) \tag{2.9}$$

J represents the ionic current densities for the different substances (Na, K, ...) (Poznanski, 2004).

The parameters for the SENN model used to model Aβ fibers can be found in Table 2.3.

Table 2.3: Standard parameters for the SENN model (Graham et al., 2019).

Parameter	Value
Fiber diameter	7.3 μm
Axon diameter at node	5.11 μm
Nodal gap	2.5 μm
Axoplasmic resistivity	100 Ωcm
External medium resistivity	300 Ωcm
Membrane capacity	2 μF/cm^2
Membrane conductivity	30,4 mS/cm^2
Internodal distance	730 μm

2.3 C fibers

As mentioned in section 1.2.2 C fibers play a significant role in understanding pain. The Sundt model is used to represent these C fibers. The Sundt model includes voltage-gated Na^+ channels and delayed rectifier K^+ channels (Sim4Life, 2020).

2.3.1 Sundt model

The mathematics behind the Sundt model are based on equations from known literature. The first parameter that has to be modelled are the voltage-gated Na^+ channels Na_v. The equations used for Na_v are adapted from (Cummins, Sheets, & Waxman, 2007), (Sheets, Jackson, Waxman, Dib-Hajj, & Cummins, 2007) and (Traub, Wong, Miles, & Michelson, 1991), shown in equations 2.10 to 2.18.

$$J_{\mathrm{Na}} = G_{\mathrm{Na}} \cdot m^3 h \cdot (V - E_{\mathrm{Na}}) \tag{2.10}$$

$$m_\infty(V) = \frac{\alpha_\mathrm{m}(V)}{\alpha_\mathrm{m}(V) + \beta_\mathrm{m}(V)} \tag{2.11}$$

$$\tau_\mathrm{m}(V) = \frac{1}{\alpha_\mathrm{m}(V) + \beta_\mathrm{m}(V)} \tag{2.12}$$

$$\alpha_\mathrm{m}(V) = 0.55\frac{7.1 - V}{e^{\frac{7.1-V}{4}}} \tag{2.13}$$

$$\alpha_\mathrm{m}(V) = 0.22e^{\frac{23-V}{18}} \tag{2.14}$$

$$h_\infty(V) = \frac{\alpha_\mathrm{h}(V)}{\alpha_\mathrm{h}(V) + \beta_\mathrm{h}(V)} \tag{2.15}$$

$$\tau_\mathrm{h}(V) = \frac{1}{\alpha_\mathrm{h}(V) + \beta_\mathrm{h}(V)} \tag{2.16}$$

$$\beta_\mathrm{m}(V) = \frac{0.48(V - 46.1)}{e^{\frac{V-46.1}{5}} - 1} \tag{2.17}$$

$$\beta_\mathrm{h}(V) = \frac{6.92}{1 + e^{\frac{46-V}{5}}} \tag{2.18}$$

The second group of parameters that have to be modelled are the K^+ delayed-rectifier channels. This is done by adapting the current conductance equations from (Borg-Graham, 1987). These are shown in equations 2.19 to 2.23.

$$J_\mathrm{K(DR)} = G_\mathrm{K(DR)} \cdot n^3 l \cdot (V - E_\mathrm{k}) \tag{2.19}$$

$$\alpha_\mathrm{n}(V) = \frac{e^{-5\times10^{-3}\cdot(V+32)\cdot9.648\times10^4}}{2562.35} \tag{2.20}$$

$$\alpha_\mathrm{l}(V) = \frac{e^{2\times10^{-3}\cdot(V+61)\cdot9.648\times10^4}}{2562.35} \tag{2.21}$$

$$\beta_\mathrm{n}(V) = \frac{e^{-2\times10^{-3}\cdot(V+32)\cdot9.648\times10^4}}{2562.35} \tag{2.22}$$

$$\beta_\mathrm{l}(V) = \frac{e^{-2\times10^{-3}\cdot(V+32)\cdot9.648\times10^4}}{2562.35} \tag{2.23}$$

The fiber diameter equals 0.8 μm and the resting potential is set to -55 mV. These fibers have a specific membrane resistivity $R_{\mathrm{m}} = 100\ \Omega cm$ and an axial resistance $R_{\mathrm{a}} = 100\ \Omega cm$.

2.4 Activating function

The activating function of a potential describes how an extracellular electric field changes the membrane potential of a neuron (Rattay, 1987) and is defined as the second derivative of the extracellular potential. When the activating function shows a high positive value it means that depolarization will occur. Consequently when this positive trend appears it is likely that an action potential fires. In contrary if the activating function shows a negative value it is highly unlikely that an action potential will fire. A negative activating function denotes hyperpolarization. Two ideal cases of activating functions will be explained as shown in Figure 2.5.

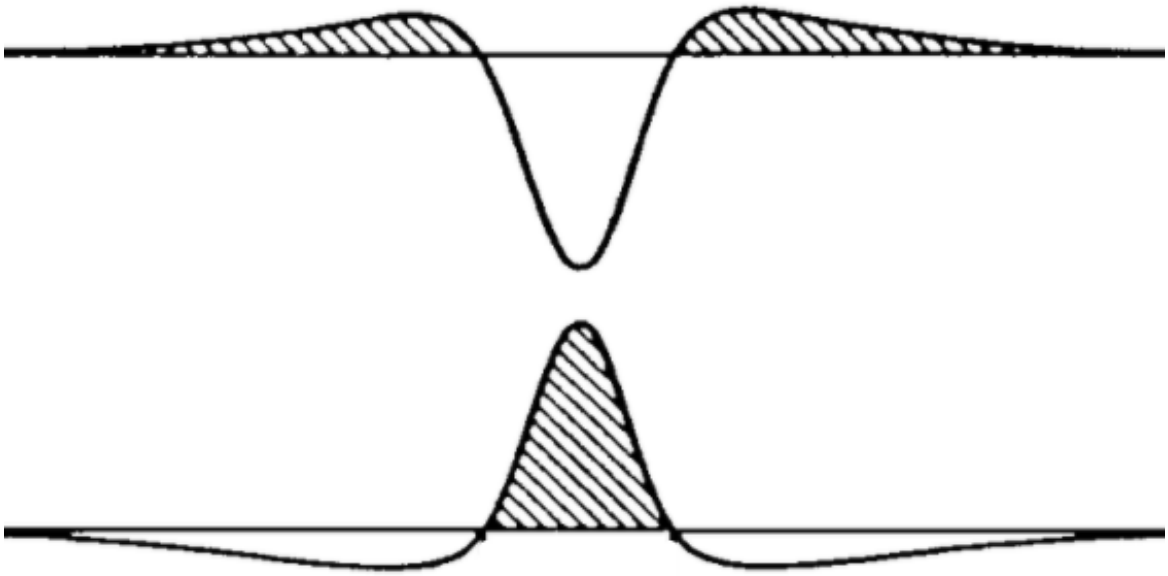

Figure 2.5: Activating function during electrical stimulation. Upper case is the activating function with anodal stimulation. Lower case is the activating function with cathodal stimulation (Rattay et al., 1987).

The case of anodal stimulation shows an activating function with a high negative value in the middle and a slightly positive value symmetrical to the sides. This means hyperpolarization will occur right under the electrode while action potentials fire at the sides propagating further away from the electrode.

In case of cathodal stimulation the activating function shows a high positive value right in the middle. It becomes clear that an action potential will fire right under the electrode.

In conclusion is the activating function used as a tool to see where the action potentials will most likely form and which regions de- or hyperpolarize.

2.5 Activation threshold

One of the main parameters to study is the activation threshold for action potential firing of the different nerve fibers in multiple stimulation configurations. This is done by setting the Dirichlet potential boundary condition of the active electrode to -1V (or 1V depending on whether cathodal or anodal stimulation is used) and the potential of the return electrode to 0V. After running the simulation, the titration factor can be derived via the analysis tab. This titration factor has to be substituted into formula 2.24 to find the excitation threshold.

$$\phi_T(t) = \phi \cdot T \cdot a(t) \tag{2.24}$$

In formula 2.24 $\phi = \mathrm{V}_{electrode}$, T is the titration factor and a(t) is the modulating pulse.

Not only the voltage is interesting regarding stimulation threshold, but also the stimulation current is from utmost importance because the stimulation current is not depended on the geometry of the electrode. To derive this stimulation current the flux evaluator is used. The flux evaluator algorithm works by computing the flux of a vector field, in this case the current density field, through a surface mesh using Formula 2.25.

$$\int\int \vec{v}\,\vec{n}\,dS \tag{2.25}$$

The calculated flux is described by the software in terms of $\frac{A}{m^2}m^2$. Consequently by selecting the electrode and the overall field the current is derived directly. Finally this current has to be scaled with the titration factor to determine the excitation threshold current.

2.6 Grid study

Sim4Life evaluates voxels, thus it is important to choose the grid of the model accordingly. By decreasing the max step value in the grid settings, more and smaller voxels will be present which results in a more accurate analysis of the data. A downside of decreasing the max step value in the grid is that more computational power is needed to evaluate these voxels. From this it becomes clear that a grid study has to be done and a balance between grid size and computational power has to be established.

In this thesis the grid study is conducted by creating a grid mask around the active and return electrode and around the axons of the different nerve fibers. The starting point of the study begins by setting the maximum step of all grid parameters (general tissue, axon and electrodes) to 0.5 mm. The boundary condition of the active electrode is set to 1 V (Dirichlet condition) and the potential of the return electrode to 0 V (Dirichlet condition). The reason for this is because the titration factors will be compared. This titration factor will be used to calculate the eventual action potential thresholds by multiplying this factor with the potential of the electrode and the modulating pulse. Subsequently one of the parameters is adapted starting by the active electrode and lowered until no change in titration factor is seen anymore. When the titration factor doesn't change anymore, it means that decreasing the grid size of that parameter has no influence and will only result in more need of computational power and consequently a longer simulation time. By doing so the grid values, visible in Table 2.4, are found. The total number of cells in the grid equals 42.258 M cells.

Table 2.4: Max step values of the grid of the DRG model

	Grid size (mm)
Active electrode	0.05
Return electrode	0.05
Axon	0.05
General tissue	0.5

2.7 Modulating pulses

In neuromodulation different pulse types can be used. It is important to study these pulses because some can have a more desirable effect on the patient than others.

The Sim4Life software allows for several different pulse types, but in this master dissertation two types are studied: monopolar and bipolar. For most of the simulations conducted in this thesis the monopolar pulse type, seen in Figure 2.6, is used.

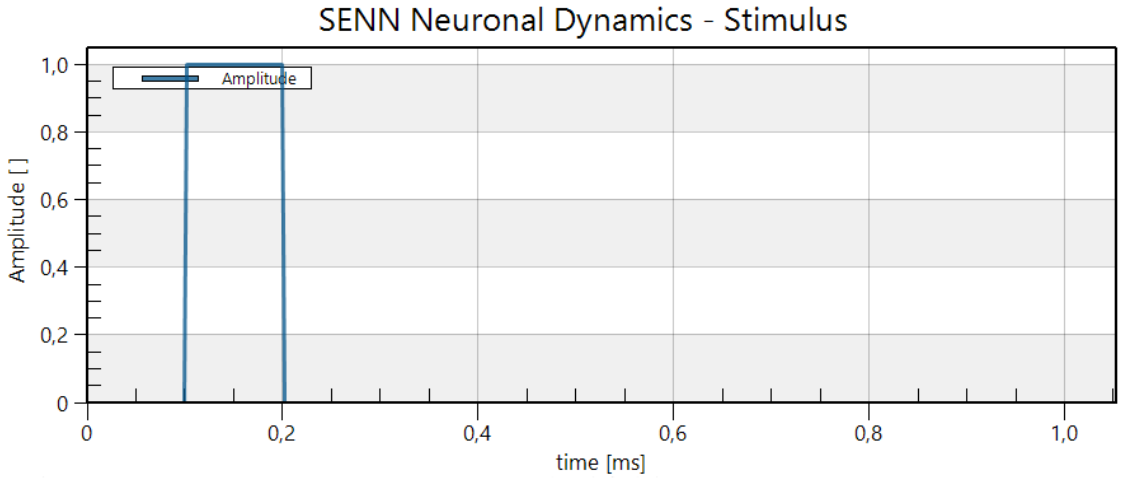

Figure 2.6: Monopolar modulation pulse type

Also the influence of a varying pulse width, in this case 0.1 ms, will be studied.

Even though most simulations in this thesis are done by using a monopolar pulse type also the bipolar pulse type, seen in Figure 2.7, is used. This is done to establish a comparison between the influence of both types.

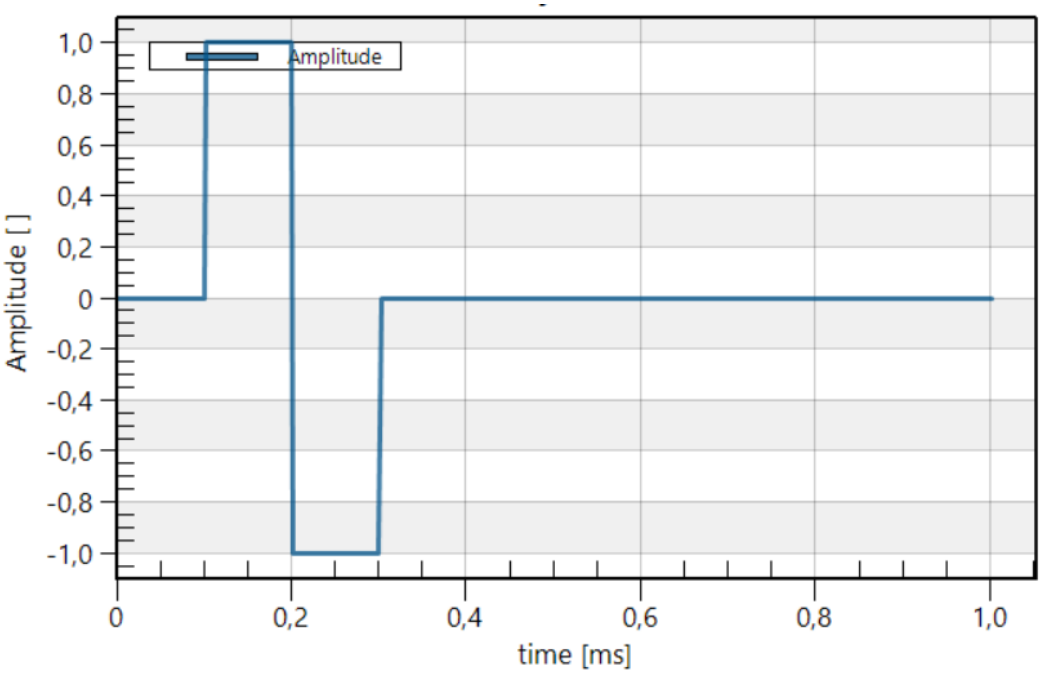

Figure 2.7: Bipolar modulation pulse type

2.8 Automation of model, simulation and analysis

Because it is very time consuming to manually create the model, perform the simulation and perform the analysis, a Python and two Matlab scripts are written.

2.8.1 Python script

The Python script allows the user to create the model and perform the simulations.

First of all the electromagnetic and neuronal models are created.

After this the electromagnetic simulation parameters are implemented such as the setup settings, material settings, boundary conditions, etc. Following this is the implementation of the neuron simulation. It is especially useful to automate this step because 39 pointsensors need to be added to one single axon to generate data such as the membrane voltage across the length of the axon.

Finally the analysis step is added to the code. It is possible in Sim4Life to extract data to a .csv file by means of the excel exporter functionality (Sim4Life, 2020). Without the python script the user has to add one of these excel exporters manually for every pointsensor along the axon. This is not feasible, consequently this process is automated for every pointsensor. Another way of exporting data in Sim4Life is by means of a Matlab exporter. As the name suggests, it exports the data to a .mat file. This is done for the electromagnetic field generated by the electrodes. Another process that is added to the python script is the extraction of the titration factor. This is the factor that allows the user to find the threshold stimulus for action potential generation.

In conclusion the python script automates the creation of the model, the execution of the simulation and the performance of some of the analysis. On top of this it also gives the user the needed data in convenient formats such as .csv and .mat files in one click.

2.8.2 Matlab scripts

Further data analysis is performed using Matlab. Two different Matlab scripts are written. The first one allows the user to manipulate the data of the electromagnetic field and the second one creates plots of the membrane potential along the axon at certain timestamps.

The first Matlab script that is written, Activation_Function.m, manipulates the electromagnetic field data, EM.mat, generated by the python script in Sim4life as described in section 2.8.1. The EM.mat file contains four arrays of data: Snapshot0, Axis0, Axis1 and Axis2. Each line of the Snapshot0 matrix contains the value of the exported field extracted from one cell of the discretised setup. The number of lines in the matrix corresponds to the number of cells in the employed field sensor. The values are stored by reading along the X-axis first, then Y, then Z. Axis0, Axis1 and Axis2 are 1-D arrays containing, respectively, the X, Y and Z coordinates of the grid lines (Sim4Life, 2020). The written Matlab script, Activating_Function.m, creates plots of the extracellular potential, the first derivative and the corresponding activating function along the axon.

The second script, Membrane_Potential.m, constructs a plot of the membrane potential along the axon. The user can choose any number of plots at different timestamps to be plotted on the figure. Most interesting is to plot the membrane potential before stimulus, during stimulus and after stimulus to study how the action potentials propagate through the axon.

Chapter 3

Results

After creating the model and running the simulation, a thorough analysis of the obtained data is performed. In these simulations the boundary conditions are specified for the electrodes in each section and the boundary condition applied to the boundaries of the simulation domain are Neumann conditions with a value equal to 0 A/m^2.

Initially the current activation thresholds are calculated for Aβ and C fibers in cathodal and anodal stimulation set-ups. Thereafter the written Matlab scripts (Activating_Function.m and Membrane_Potential.m) are used to determine information about the activating functions and the membrane potentials of the models and corresponding simulations.

After determining the membrane potentials and activating functions, the influences of different parameters are studied. The first parameter that is examined is the influence of the axon location within the DRG on the simulations. Whether the axon is located closer to or further away from the electrode shaft could probably have a significant impact on the excitation thresholds and the times of first spike. When talking about the position of the axon along the Z-axis, what is meant is moving the axon closer or further away from the electrode shaft as shown in Figure 3.1 with the coordinate system shown in the left bottom corner. The next parameter that is studied is the pulse length followed by the pulse type. Using a monophasic versus a biphasic pulse and varying the pulse length could possibly have an influence on the activation thresholds as well. The final parameter that is researched is the axon diameter. These diameters can vary and consequently also impact the results. The results generated by studying these parameters are described in the sections below.

Finally stimulation of a nerve fiber bundle is performed. The aim of studying this

nerve bundle is to determine the influence of the distance between the electrode and the DRG on the percentage of activated nerve fibers.

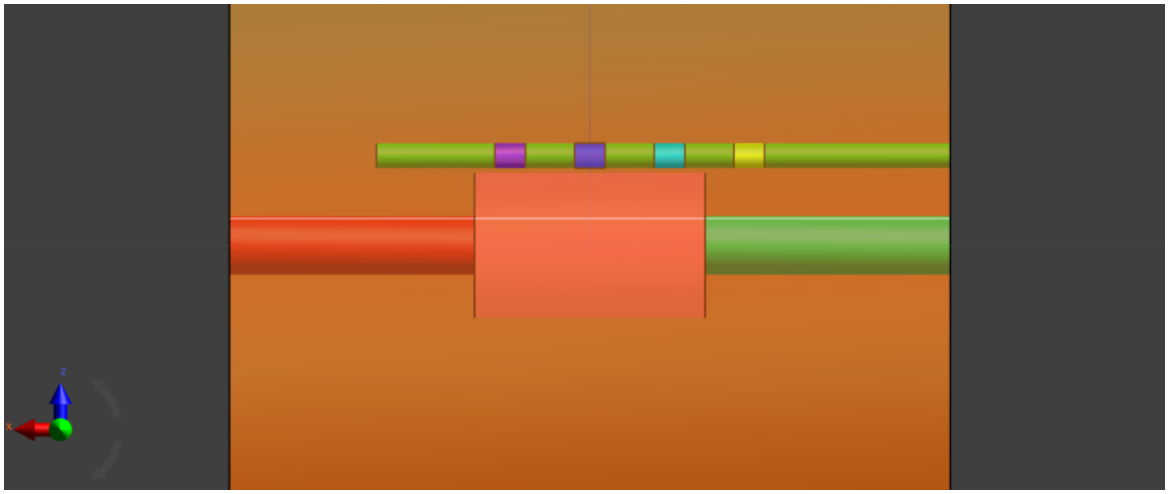

Figure 3.1: Position of the axon (white line) in the DRG model.

3.1 Cathodal stimulation of Aβ fibers

This section is dedicated to the stimulation of Aβ fibers by using cathodal stimulation. Cathodal stimulation means that the Dirichlet condition on the active electrode is set to -1 V (cathode) and the Dirichlet condition on the return electrode is set to 0 V (anode).

3.1.1 Activation threshold for Aβ fibers stimulated by cathodal stimulation

The first part that is studied is the activation threshold for action potential firing in the Aβ neuron fibers. A monophasic modulating pulse is used which can be seen in Figure 2.6. The calculation of the excitation threshold is done by determining the titration factor and using Formula 2.24 as described in section 2.5. By using the flux evaluator, as also described in section 2.5, the excitation threshold current can be calculated. In this case the excitation threshold current equals 0.39 mA.

3.1.2 Activating function of Aβ fibers stimulated by cathodal stimulation

The next step is to look at the activating function. The activating function is calculated from the EM.mat file generated by Sim4Life. This EM.mat file is processed by

the Activating_Function.m script as described in section 2.8.2. The script calculates and plots the external potential, the first derivative and the second derivative (or activating function) of the external potential. The respective plot is shown in Figure 3.2.

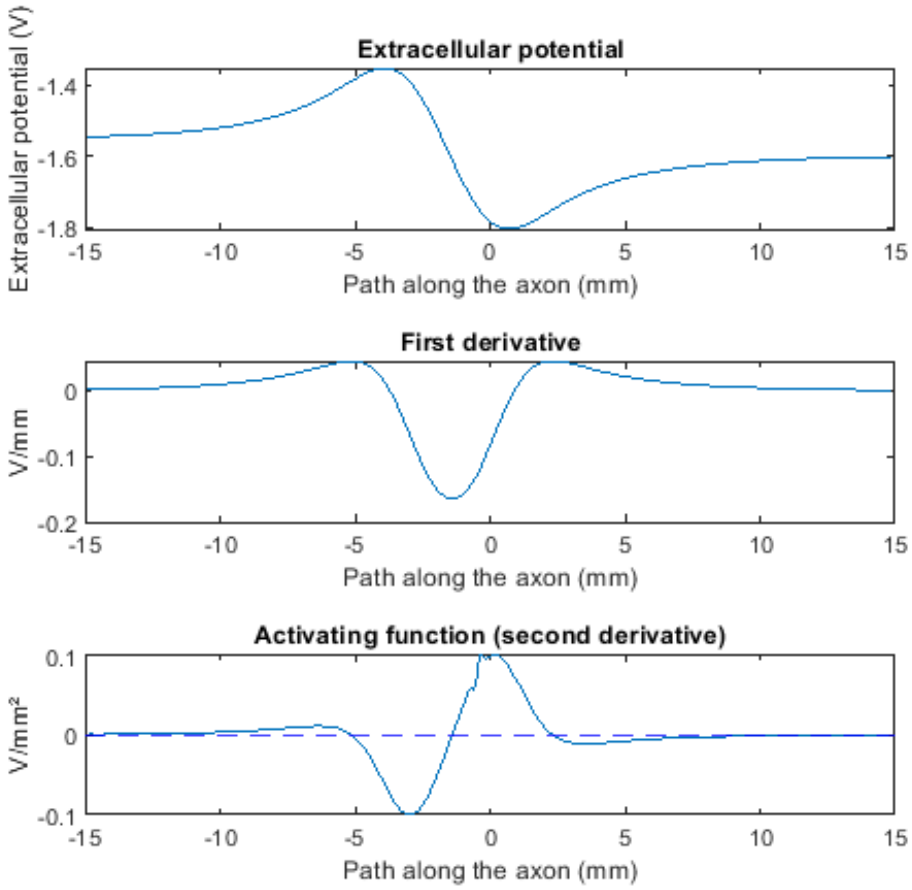

Figure 3.2: The external potential, first derivative and activating function in cathodal stimulation of Aβ fibers with the active electrode positioned above the center of the DRG.

The activating function of cathodal stimulation is not of the form presented in section 2.4. The reason is that this is actually a superposition of two activating functions: the one generated by the active electrode (cathode) and the one generated by the return electrode (anode). Consequently a high positive peak is shown at 0 mm coming from the positive peak under the cathode as would be in cathodic stimulation and the small positive peak coming from the anode as expected in anodal stimulation. This results in a high positive peak at 0 mm. The significant negative peak is coming from the anode which is positioned at the location of this negative peak and the small negative bump created by the cathode.

The activating function is used as a tool to estimate where an action potential will occur. As described in section 2.4 the high positive peak means that depolarization will most likely take place at 0 mm, the location under the active electrode which acts as a cathode. The negative peak means that hyperpolarization will occur to the left of the center, the location under the return electrode which acts as an anode. The next step is to compare this activating function with the actual membrane potential of the Aβ fiber.

3.1.3 Membrane potential of Aβ fibers stimulated by cathodal stimulation

By looking at the activating function, seen in Figure 3.2, it becomes clear that an action potential will probably originate right underneath the activate electrode. By running the Membrane_Potential.m script, described in subsection 2.8.2, the membrane potential in function of the path along the axon is calculated and plotted for different timestamps as shown in Figure 3.3.

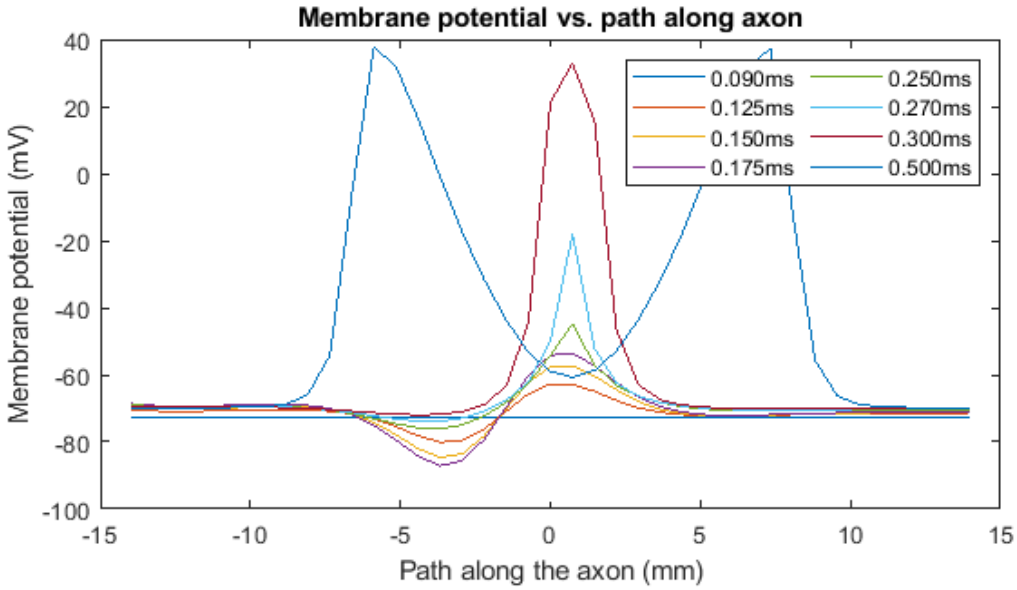

Figure 3.3: Membrane potential of Aβ fibers when performing cathodal stimulation with the active electrode right above the DRG in function of path along the axon for different timestamps.

Figure 3.3 shows that right before stimulation (0.090ms) the potential is close to the resting potential and right after stimulation (0.125ms) a positive trend arises around 0mm. This is the beginning of the action potential which keeps on growing centrally until it propagates to the sides at later timestamps. Hyperpolarization occurs to

the left of the center. These findings confirm what was estimated by the activating function.

3.1.4 Influence of axon location on the excitation threshold of Aβ fibers when stimulated by cathodal stimulation

After generating the results mentioned above it is important to study the influence of certain parameters to get a better understanding of the behaviour of Aβ fibers subjected to DRGS. The first parameter that is studied is the position of the axon within the DRG.

To study this influence five different axon positions are chosen: one in the middle of the DRG and the others 1.09 mm and 0.545 mm upwards or downwards along the Z-axis. The results of these simulations when the Aβ fibers are subjected to cathodal stimulation with a monophasic pulse (pulse width equal to 0.1 ms) can be seen in Table 3.1.

Table 3.1: Influence of the position along the Z-axis of Aβ nerve fibers on the time of first spike and the excitation threshold current when subjected to cathodal stimulation with a monophasic pulse (pulse width equal to 0.1 ms).

Axon position along the Z-axis (mm)	**Location of first spike (mm)**	**Time of first spike (ms)**	**Excitation threshold current (mA)**
1,090	0,000	0,265	0,15
0,545	0,000	0,270	0,25
0,000	0,735	0,278	0,39
-0,545	0,735	0,270	0,58
-1,090	0,735	0,283	0,85

From Table 3.1 it becomes clear that the threshold to activate Aβ fibers increases if the fibers are located further away from the active electrode and vice versa. When the axon is closest to the active electrode the excitation threshold current is the lowest and equals 0.15 mA. When the axon is positioned furthest away from the active electrode the excitation threshold current equals 0.85 mA. This was expected because the electrical field will be more intense closer to the electrode. These results for the current excitation thresholds are between clinical ranges (< 1 mA) (Deer et al., 2017). This is a first indicator that Aβ fibers are directly stimulated by DRGS in a clinical

setting according to this model.

The time of first spike doesn't change significantly and remains between 0.265 and 0.283 ms.

The location of first spike remains at 0 mm along the axon for the fibers located at 1.09 and 0.545 mm, but changes to 0.735 mm for the fibers located at 0, -0.545 and -1.09 mm. This is due to the influence of the return electrode which is acting like an anode.

3.1.5 Influence of stimulation pulse length and stimulation pulse type for cathodal stimulation of Aβ fibers

The stimulation pulse used until this point was always monophasic and had a duration of 0.1 ms as shown Figure 2.6. First of all the influence of the modulating pulse width is studied. Pulse widths of respectively 0.1 ms, 0.2 ms, 0.3 ms, 0.4 ms and 0.5 ms are used. The influence of these different pulse widths on the Aβ fibers are shown in respectively Table 3.2 to Table 3.5. Note that the results for a modulating pulse of 0.1 ms are already shown in Table 3.1.

Table 3.2: Influence of stimulating Aβ fibers with cathodal stimulation using a monophasic pulse with a pulse width of 0.2 ms on the location of first spike, time of first spike and excitation threshold current for different positions of the fibers along the Z-axis.

Axon position along the Z-axis (mm)	**Location of first spike (mm)**	**Time of first spike (ms)**	**Excitation threshold current (mA)**
1,090	0,000	0,353	0,11
0,545	0,735	0,358	0,18
0,000	0,735	0,368	0,29
-0,545	0,735	0,403	0,43
-1,090	0,735	0,365	0,62

Table 3.3: Influence of stimulating Aβ fibers with cathodal stimulation using a monophasic pulse with a pulse width of 0.3 ms on the location of first spike, time of first spike and excitation threshold current for different positions of the fibers along the Z-axis.

Axon position along the Z-axis (mm)	**Location of first spike (mm)**	**Time of first spike (ms)**	**Excitation threshold current (mA)**
1,090	0,000	0,455	0,10
0,545	0,735	0,450	0,17
0,000	0,735	0,443	0,26
-0,545	0,735	0,465	0,39
-1,090	0,735	0,443	0,56

Table 3.4: Influence of stimulating Aβ fibers with cathodal stimulation using a monophasic pulse with a pulse width of 0.4 ms on the location of first spike, time of first spike and excitation threshold current for different positions of the fibers along the Z-axis.

Axon position along the Z-axis (mm)	**Location of first spike (mm)**	**Time of first spike (ms)**	**Excitation threshold current (mA)**
1,090	0,000	0,515	0,10
0,545	0,735	0,535	0,16
0,000	0,735	0,540	0,25
-0,545	0,735	0,540	0,37
-1,090	0,735	0,560	0,54

Table 3.5: Influence of stimulating Aβ fibers with cathodal stimulation using a monophasic pulse with a pulse width of 0.4 ms on the location of first spike, time of first spike and excitation threshold current for different positions of the fibers along the Z-axis.

Axon position along the Z-axis (mm)	**Location of first spike (mm)**	**Time of first spike (ms)**	**Excitation threshold current (mA)**
1,090	0,000	0,565	0,10
0,545	0,735	0,600	0,16
0,000	0,735	0,698	0,25
-0,545	0,735	0,678	0,37
-1,090	0,735	0,645	0,53

When looking at these results presented above it becomes clear that if the pulse width is increased the first spike will be consistently later and vice versa and the excitation thresholds will be lower. Note that the decrease in excitation threshold gets less significant when the values for the pulse width are higher. The location of first spike appears to be independent of pulse width.

Until now all simulations are done using a monophasic stimulation pulse. As described in section 2.7 there are different types of stimulation pulses. In the context of this thesis two types of pulses will be examined: monophasic and biphasic. These pulse types can respectively be seen in Figure 2.6 and Figure 2.7.

The influence on the times of first spike and the excitation threshold currents are studied when using a biphasic pulse with the cathodal phase first followed by the anodal phase instead of a monophasic pulse. These results are shown in Table 3.6.

Table 3.6: Influence of stimulating Aβ fibers using a biphasic pulse with first the cathodal and second the anodal phase with a pulse width of 0.1 ms for each phase on the location of first spike, time of first spike and excitation threshold current for different positions of the fibers along the Z-axis.

Axon position along the Z-axis (mm)	**Location of first spike (mm)**	**Time of first spike (ms)**	**Excitation threshold current (mA)**
1,090	0,000	0,250	0,16
0,545	0,000	0,243	0,26
0,000	0,735	0,243	0,41
-0,545	0,735	0,260	0,61
-1,090	0,735	0,243	0,91

From Table 3.6 it becomes clear that, similar to using a monophasic pulse, the excitation thresholds tend to get higher when moving the axon further away from the DRG and vice versa. The activation threshold current when the axon is positioned closest to the electrode equals 0.16 mA and when positioned furthest away from the electrodes 0.91 mA. These threshold currents are higher than for monophasic stimulation. The times of first spike remain in close proximity to each other and the locations of first spike follow the same trend as for monophasic stimulation with a pulse width of 0.1ms.

3.1.6 Influence of axon diameter when stimulating $A\beta$ fibers by cathodal stimulation

According to literature the diameter of Aβ fibers varies between 5 - 12 μm (Manzano, Giuliano, & Nóbrega, 2008). The diameter chosen in the simulations done until now was 7.3 μm. The thickness of the nerve fiber will also have a certain influence on the results. To study this influence different thicknesses of fibers have been chosen varying from 5.3 - 11.3 μm. The influence on the activation thresholds and times of first spike are shown in Table 3.7.

Table 3.7: Influence of the axon diameter on the time of first spike and excitation threshold current when performing cathodal stimulation on an Aβ fiber positioned in the center of the DRG using a monophasic pulse with a pulse width of 0.1 ms.

Axon diameter (μm)	**Time of first spike (ms)**	**Excitation threshold current (mA)**
5,3	0,283	0,63
6,3	0,273	0,48
7,3	0,278	0,39
8,3	0,278	0,32
9,3	0,355	0,28
10,3	0,275	0,25
11,3	0,260	0,23

These results show that the excitation threshold current decreases when the axon diameter increases and the times of first spike remain approximately the same.

3.2 Anodal stimulation of Aβ fibers

In this section all simulations are performed by anodal stimulation of Aβ fibers. The Dirichlet condition put on the active electrode is now positive and equals 1 V, consequently the active electrode will now act as an anode. The Dirichlet condition on the return electrode equals 0 V, meaning that the return electrode will now act as a cathode.

3.2.1 Activation threshold for Aβ fibers stimulated by anodal stimulation

The activation threshold for anodal stimulation of Aβ fibers is found by using the same methodology as described in Section 2.4. By doing so it becomes clear that the current excitation threshold equals 0,39 mA. This is the same as for cathodal stimulation. This is due to the fact that the anode and cathode just shifted places resulting in a different location of first spike.

3.2.2 Activating function of Aβ fibers stimulated by anodal stimulation

The activating function is again calculated by using the written Matlab script Activating_Function.m. The respective plot can be seen in Figure 3.4.

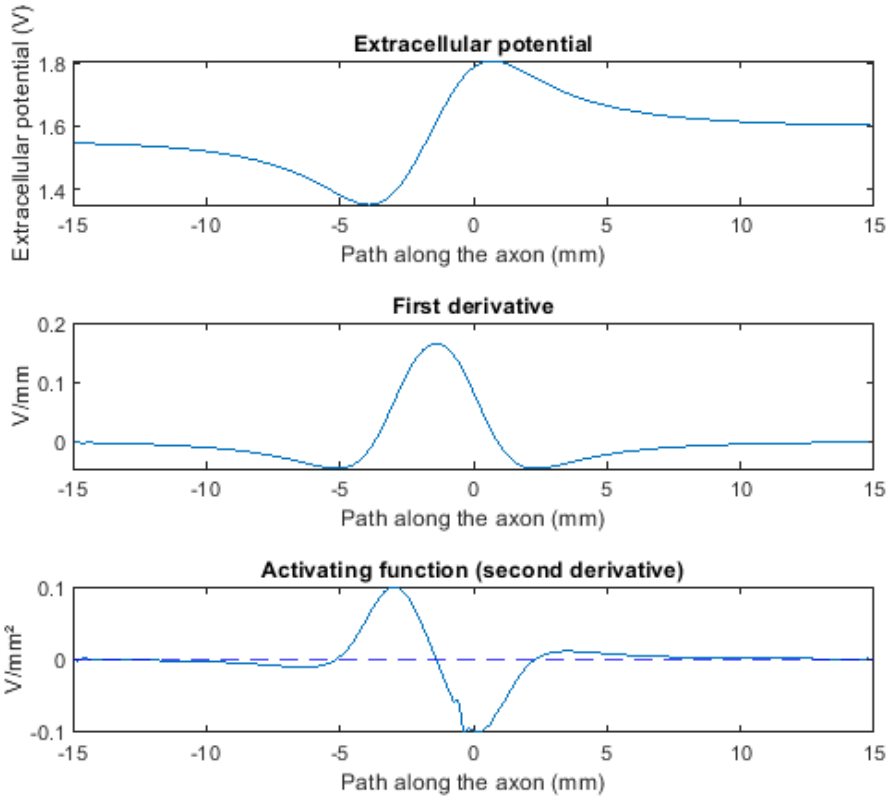

Figure 3.4: The external potential, first derivative and activating function in anodal stimulation of Aβ fibers with the active electrode positioned above the center of the DRG.

Anodal stimulation is the opposite of cathodal stimulation, thus the potential applied to the active electrode is now positive. The expected result should be that the activating function for anodal stimulation is a mirroring, around the X-axis, of the activating function for cathodal stimulation. When studying the activating function it becomes clear that this is true. Again the shape of the activating function can be explained by the fact that this is a superposition of the activating function for anodal and cathodic stimulation. The negative peak at 0 mm comes from the significant negative peak in anodal stimulation by the active electrode (anode) and also from the small bump supplied by the return electrode (cathode). The significant positive peak is coming from the high positive peak in cathodic stimulation supplied by the return electrode (cathode) and the small positive bump supplied by the active electrode (anode).

Subsequently hyperpolarization will most likely occur right underneath the active electrode (0mm) and depolarization will occur not far from the center to the left resulting in an AP.

3.2.3 Membrane potential of Aβ fibers when stimulated by anodal stimulation

By running the Membrane_Potential.m script on the data acquired, the membrane potential plot of anodal stimulated Aβ fibers for different timestamps is derived. This plot can be seen in Figure 3.5. The membrane potential plot is according to the activating function, shown in Figure 3.4. The action potential originates to the left of the center. Right underneath the active electrode hyperpolarization occurs as predicted by the activating function.

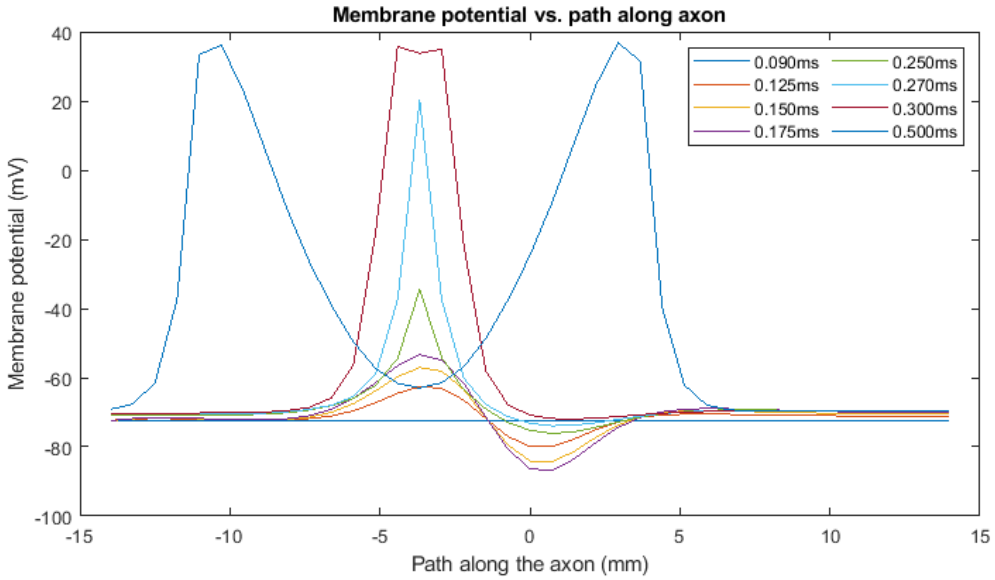

Figure 3.5: Membrane potential of Aβ-fibers when performing anodal stimulation with the active electrode right above the DRG in function of path along the axon for different timestamps.

3.2.4 Influence of axon location on the excitation threshold of Aβ fibers when stimulated by cathodal stimulation

When using anodal stimulation the same results are generated as for cathodal stimulation. The influence of the axon location on the location of first spike, time of first spike and the excitation threshold current is the first parameter that is studied. By

varying the axon position along the Z-axis (1.09 mm, 0.545 mm, 0 mm, -0.545 mm and -1.09 mm), results are generated as shown in Table 3.8.

Table 3.8: Influence of the position along the Z-axis of Aβ nerve fibers on the time of first spike and the excitation threshold current when subjected to anodal stimulation with a monophasic pulse (pulse width equal to 0.1 ms).

Axon position along the Z-axis (mm)	**Location of first spike (mm)**	**Time of first spike (ms)**	**Excitation threshold current (mA)**
1.090	-2.940	0.265	0.15
0.545	-3.675	0.305	0.25
0.000	-3.675	0.263	0.39
-0.545	-3.675	0.275	0.58
-1.09.	-3.675	0.270	0.86

From Table 3.8 it becomes clear that the same trend occurs for anodal stimulation as for cathodal stimulation. The excitation threshold increases when moving further away from the electrode. When the axon is located at 1.09 mm along the Z-axis (closest to the electrode) the excitation threshold is 0.15 mA and when the axon is located at -1.09 mm along the Z-axis (furthest away from the electrode) the excitation threshold equals 0.86 mA.

3.2.5 Influence of stimulation pulse length and stimulation pulse type for anodal stimulation of Aβ fibers

The next step is to study the influence of the stimulation pulse length when anodal stimulation is used. The stimulating pulse is varied between 0.1 ms and 0.5 ms. The results can be seen in respectively Table 3.9 to 3.12

Table 3.9: Influence of stimulating Aβ fibers with anodal stimulation using a monophasic pulse with a pulse width of 0.2 ms on the location of first spike, time of first spike and excitation threshold current for different positions of the fibers along the Z-axis.

Axon position along the Z-axis (mm)	**Location of first spike (mm)**	**Time of first spike (ms)**	**Excitation threshold current (mA)**
1.090	-2.940	0.353	0.11
0.545	-3.675	0.365	0.18
0.000	-3.675	0.358	0.29
-0.545	-3.675	0.353	0.43
-1.090	-3.675	0.365	0.63

Table 3.10: Influence of stimulating Aβ fibers with anodal stimulation using a monophasic pulse with a pulse width of 0.3 ms on the location of first spike, time of first spike and excitation threshold current for different positions of the fibers along the Z-axis.

Axon position along the Z-axis (mm)	**Location of first spike (mm)**	**Time of first spike (ms)**	**Excitation threshold current (mA)**
1,090	-3.675	0,438	0,10
0,545	-3.675	0,438	0,17
0,000	-3.675	0,440	0,26
-0,545	-3.675	0,430	0,39
-1,090	-3.675	0,440	0,57

Table 3.11: Influence of stimulating Aβ fibers with anodal stimulation using a monophasic pulse with a pulse width of 0.4 ms on the location of first spike, time of first spike and excitation threshold current for different positions of the fibers along the Z-axis.

Axon position along the Z-axis (mm)	**Location of first spike (mm)**	**Time of first spike (ms)**	**Excitation threshold current (mA)**
1,090	-3.675	0,555	0,10
0,545	-3.675	0,525	0,16
0,000	-3.675	0,538	0,25
-0,545	-3.675	0,525	0,38
-1,090	-3.675	0,538	0,54

Table 3.12: Influence of stimulating Aβ fibers with anodal stimulation using a monophasic pulse with a pulse width of 0.5 ms on the location of first spike, time of first spike and excitation threshold current for different positions of the fibers along the Z-axis.

Axon position along the Z-axis (mm)	**Location of first spike (mm)**	**Time of first spike (ms)**	**Excitation threshold current (mA)**
1,090	-3.675	0,603	0,10
0,545	-3.675	0,593	0,16
0,000	-3.675	0,573	0,25
-0,545	-3.675	0,618	0,37
-1,090	-3.675	0,613	0,54

The same conclusion can be drawn as for cathodal stimulation namely: when the pulse width is smaller the activation thresholds will be higher and vice versa. Also the first spike will occur faster when choosing the pulse width lower and vice versa.

The next parameter to study is the influence of a biphasic pulse instead of a monophasic pulse. The influence of this biphasic pulse, consisting of first the anodal phase and second the cathodal phase (with a pulse width of 0.1 ms for each phase), on the location of the first spike, time of first spike and the excitation thresholds when using a modulating pulse of 0.1ms can be seen in Table 3.13.

Table 3.13: Influence of stimulating Aβ fibers using a biphasic pulse with first the anodal and second the cathodal phase with a pulse width for each phase of 0.1 ms for each phase on the location of first spike, time of first spike and excitation threshold current for different positions of the fibers along the Z-axis.

Axon position along the Z-axis (mm)	**Location of first spike (mm)**	**Time of first spike (ms)**	**Excitation threshold current (mA)**
1,090	-2.940	0,275	0,16
0,545	-3.675	0,255	0,26
0,000	-3.675	0,253	0,41
-0,545	-3.675	0,268	0,61
-1,090	-3.675	0,260	0,91

Table 3.13 shows the same trend as for monophasic stimulation. When moving the axon closer to the electrodes the excitation threshold current will be lower and vice versa. Also the times of first spike remain close to each other.

3.2.6 Influence of axon diameter when stimulating Aβ fibers by anodal stimulation

Similar to the process done for cathodal stimulation the axon diameter is studied and varied between 5.3 and 11.3 μm. The influence of the diameter on the time of first spike and the excitation threshold can be seen in Table 3.14.

Table 3.14: Influence of the axon diameter on the time of first spike and excitation threshold current when performing anodal stimulation on an Aβ fiber positioned in the middle of the DRG using a monophasic pulse with a pulse width of 0.1ms.

Axon diameter (μm)	**Time of first spike (ms)**	**Excitation threshold current (mA)**
5,3	0,275	0,63
6,3	0,268	0,48
7,3	0,263	0,39
8,3	0,280	0,32
9,3	0,263	0,28
10,3	0,295	0,25
11,3	0,265	0,22

From Table 3.14 it becomes clear that similar to cathodal stimulation increasing the diameter of the nerve fibers decreases the excitation threshold current and vice versa. The values for the times of first spike remain close proximity to each other.

3.3 Cathodal stimulation of C fibers

Besides the SENN model for modelling heavily myelinated Aβ fibers, Sim4Life also offers a Sundt model to model unmyelinated C fibers as described in section 2.3.1. These fibers also play an important role in understanding pain, hence the following sections are dedicated to the study of C fibers starting with cathodal stimulation. The boundary conditions of the electrodes are the same as in cathodal stimulation of Aβ fibers (-1 V on the active electrode and 0 V on the return electrode).

3.3.1 Activation threshold for C fibers stimulated by cathodal stimulation

The activation threshold for C fibers stimulated by cathodal stimulation with the active electrode above the center of the DRG is determined using the same methodology as previously introduced for Aβ fibers. After running the Sim4Life simulation, using the flux evaluator and scaling this value with the titration factor, the excitation threshold current becomes 132.61 mA. Naturally this value of stimulation current will never be applied in clinical settings because this could harm the patient. The excitation threshold not being within clinical ranges could be a first indication that C fibers are not stimulated when applying DRGS according to this model.

3.3.2 Activating function of C fibers stimulated by cathodal stimulation

The activating function is calculated from the electric field emitted by the electrodes. Consequently it is expected that the activating function is the same as for cathodal stimulation of Aβ fibers, but scaled differently as the excitation threshold is much higher than for Aβ fibers. The corresponding activating function is shown in Figure 3.6. Hence the membrane potential will be the same but more current will be needed to activate these C fibers.

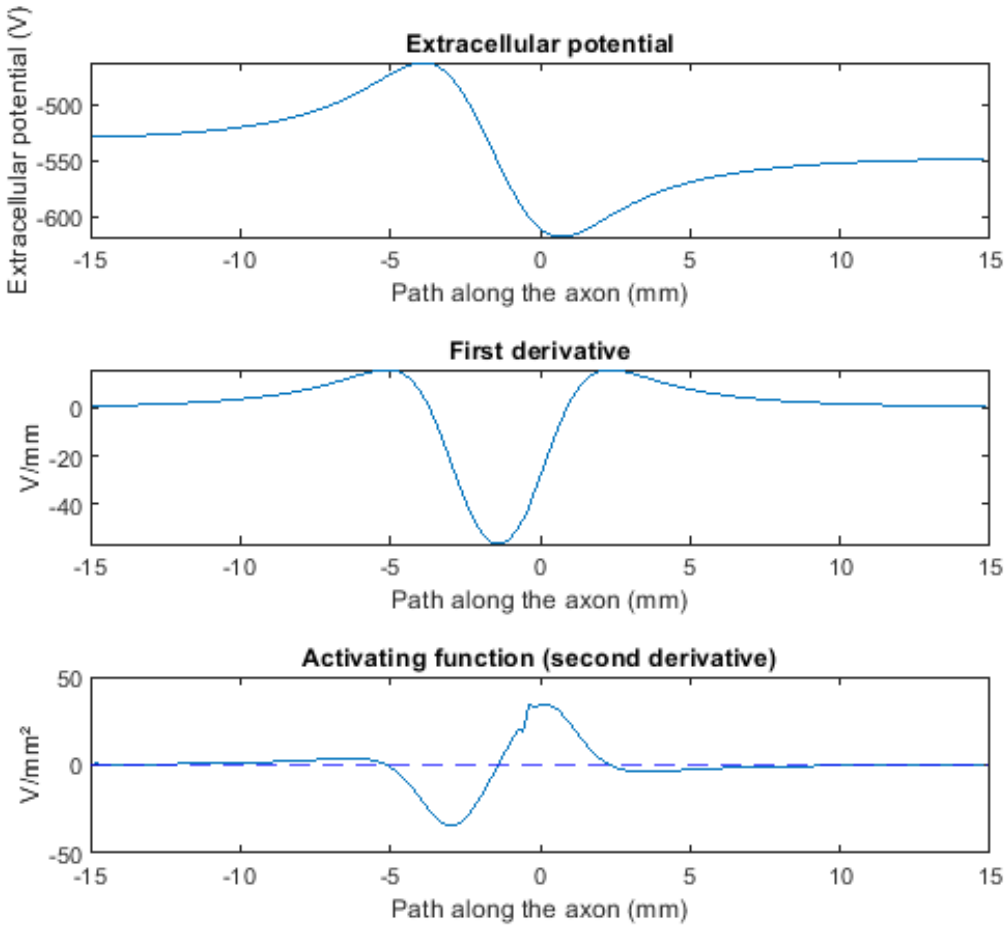

Figure 3.6: The external potential, first derivative and activating function in cathodal stimulation of C fibers with the active electrode positioned above the center of the DRG.

3.3.3 Influence of axon location on the excitation threshold of C fibers when stimulated by cathodal stimulation

Next the influence of the axon location along the Z-axis of the model on the location of first spike, time of first spike and excitation threshold is determined. These results are shown in Figure 3.15 for a monophasic pulse with a pulse width equal to 0.1 ms.

Table 3.15: Influence of the position along the Z-axis of C nerve fibers on the time of first spike and the excitation threshold current when subjected to cathodal stimulation with a monophasic pulse (pulse width equal to 0.1 ms).

Axon position along the Z-axis (mm)	**Location of first spike (mm)**	**Time of first spike (ms)**	**Excitation threshold current (mA)**
1,090	-0,05	0,495	44.94
0,545	-0,05	0,4925	79.57
0,000	0,15	0,495	132.61
-0,545	0,25	0,4975	210.21
-1,090	0,45	0,495	320.23

Table 3.15 shows the same trend as in Aβ fibers namely that the excitation threshold increases when the axon is located further away from the electrode. Note that even if the axon is located closest to the electrode (1.09 mm), the excitation threshold current is still far from within the clinical range of 1 mA (44.94 mA). The location of first spike is as expected around the 0 mm point (under the cathode). The times of first spike are close to each other around 0.495 ms.

3.3.4 Influence of stimulation pulse width and stimulation pulse type for cathodal stimulation of C fibers

After assessing the influence of the axon location on the excitation threshold of the C fibers, the influence of the pulse width is determined. The pulse width is again varied between 0.1 to 0.5 ms for a monophasic pulse. These results are shown in Table 3.16 to 3.19. Note that the results for a modulation pulse width of 0.1 ms are already shown in Table 3.15.

Table 3.16: Influence of stimulating C fibers with cathodal stimulation using a monophasic pulse with a pulse width of 0.2 ms on the location of first spike, time of first spike and excitation threshold current for different positions of the fibers along the Z-axis.

Axon position along the Z-axis (mm)	**Location of first spike (mm)**	**Time of first spike (ms)**	**Excitation threshold current (mA)**
1,090	-0,05	0,563	22.35
0,545	0,00	0,563	39.54
0,000	0,10	0,560	66.31
-0,545	0,25	0,560	105.11
-1,090	0,40	0,568	159.13

Table 3.17: Influence of stimulating C fibers with cathodal stimulation using a monophasic pulse with a pulse width of 0.3 ms on the location of first spike, time of first spike and excitation threshold current for different positions of the fibers along the Z-axis.

Axon position along the Z-axis (mm)	**Location of first spike (mm)**	**Time of first spike (ms)**	**Excitation threshold current (mA)**
1,090	-0,10	0,623	15.35
0,545	0,00	0,628	27.01
0,000	0,15	0,628	45.19
-0,545	0,20	0,628	71.71
-1,090	0,40	0,630	109.04

Table 3.18: Influence of stimulating C fibers with cathodal stimulation using a monophasic pulse with a pulse width of 0.4 ms on the location of first spike, time of first spike and excitation threshold current for different positions of the fibers along the Z-axis.

Axon position along the Z-axis (mm)	**Location of first spike (mm)**	**Time of first spike (ms)**	**Excitation threshold current (mA)**
1,090	-0,10	0,683	11.91
0,545	0,00	0,683	21.00
0,000	0,15	0,683	35.12
-0,545	0,20	0,680	55.99
-1,090	0,40	0,683	84.97

Table 3.19: Influence of stimulating C fibers with cathodal stimulation using a monophasic pulse with a pulse width of 0.5 ms on the location of first spike, time of first spike and excitation threshold current for different positions of the fibers along the Z-axis.

Axon position along the Z-axis (mm)	**Location of first spike (mm)**	**Time of first spike (ms)**	**Excitation threshold current (mA)**
1,090	-0,10	0,728	10.01
0,545	-0,05	0,728	17.68
0,000	0,10	0,730	29.47
-0,545	0,20	0,733	46.66
-1,090	0,40	0,730	71.22

From these results the same conclusion as for cathodal stimulation of Aβ fibers can be drawn. The excitation threshold decreases when the pulse width increases. Note that these excitation threshold values are all outside clinical ranges of DRGS with the lowest value equal to 10.01 mA, again suggesting that C fibers are not directly stimulated when performing DRGS. The location of first spike are still around the 0 mm point and the times of first spike increases if the pulse width is increased and vice versa.

The next simulation that is performed is with a biphasic pulse instead of a monophasic pulse. This biphasic pulse starts with the cathodal phase followed by the anodal phase with a pulse width of 0.1 ms for each phase. The respective results can be seen

in Table 3.20.

Table 3.20: Influence of stimulating C fibers using a biphasic pulse with first the cathodal and second the anodal phase with a pulse width of 0.1 ms for each phase on the location of first spike, time of first spike and excitation threshold current for different positions of the fibers along the Z-axis.

Axon position along the Z-axis (mm)	**Location of first spike (mm)**	**Time of first spike (ms)**	**Excitation threshold current (mA)**
1,090	-0,10	0,2	151.27
0,545	-0,05	0,2	269.15
0,000	0,05	0,2	451.86

Table 3.20 shows that when using this biphasic pulse the lowest threshold equals 151.27 mA. This is again far outside the clinical range of 1 mA. Note that the results for -0.545 mm and -1.09 mm are not included because in these results the titration factor got so high that the terminals were stimulated instead of the correct place where the action potential would form. Because these values are so far from clinical ranges it had no further value to generate these results, hence they are not included.

3.3.5 Influence of axon diameter when stimulating C fibers by cathodal stimulation

The unmyelinated C fibers are a lot smaller than the heavily myelinated Aβ fibers. Their diameter varies between 0.2-1.5 μm (Dale Purves, 2001). Three different diameters are studied 0.2 μm, 0.8 μm and 1.5 μm. The results can be seen in Table 3.21.

Table 3.21: Influence of the axon diameter on the time of first spike and excitation threshold current when performing cathodal stimulation on a C fiber positioned in the middle of the DRG using a monophasic pulse with a pulse width of 0.1ms.

Axon diameter (μm)	**Time of first spike (ms)**	**Excitation threshold current (mA)**
0,2	0,493	526.51
0,8	0,495	224.96
1,5	0,490	71.71

From Table 3.21 it becomes clear that if the diameter increases the threshold decreases. The times of first spike remain approximately the same.

3.4 Anodal stimulation of C fibers

Finally anodal stimulation is performed with the active electrode acting as an anode and the return electrode acting as a cathode. In these simulations the Dirichlet boundary condition of the active electrode equals 1 V and the Dirichlet boundary condition of the return electrode equals 0 V.

3.4.1 Activation threshold for C fibers stimulated by anodal stimulation

The activation threshold for C fibers stimulated by anodal stimulation with the active electrode right above the DRG is determined using the same methodology as previously introduced for Aβ fibers. When using the flux evaluator and scaling this value with the titration factor, the excitation threshold current becomes 132.61 mA. This is outside the clinical range of 0.1 mA. This is the same value as for cathodal stimulation. Again this is due to the fact that the anode and cathode just switched.

3.4.2 Activating function of C fibers stimulated by anodal stimulation

The activating function of C fibers stimulated by anodal stimulation are expected to again be the same for anodal stimulation of Aβ fibers, but scaled with the new titration factor. The result can be seen in Figure 3.7.

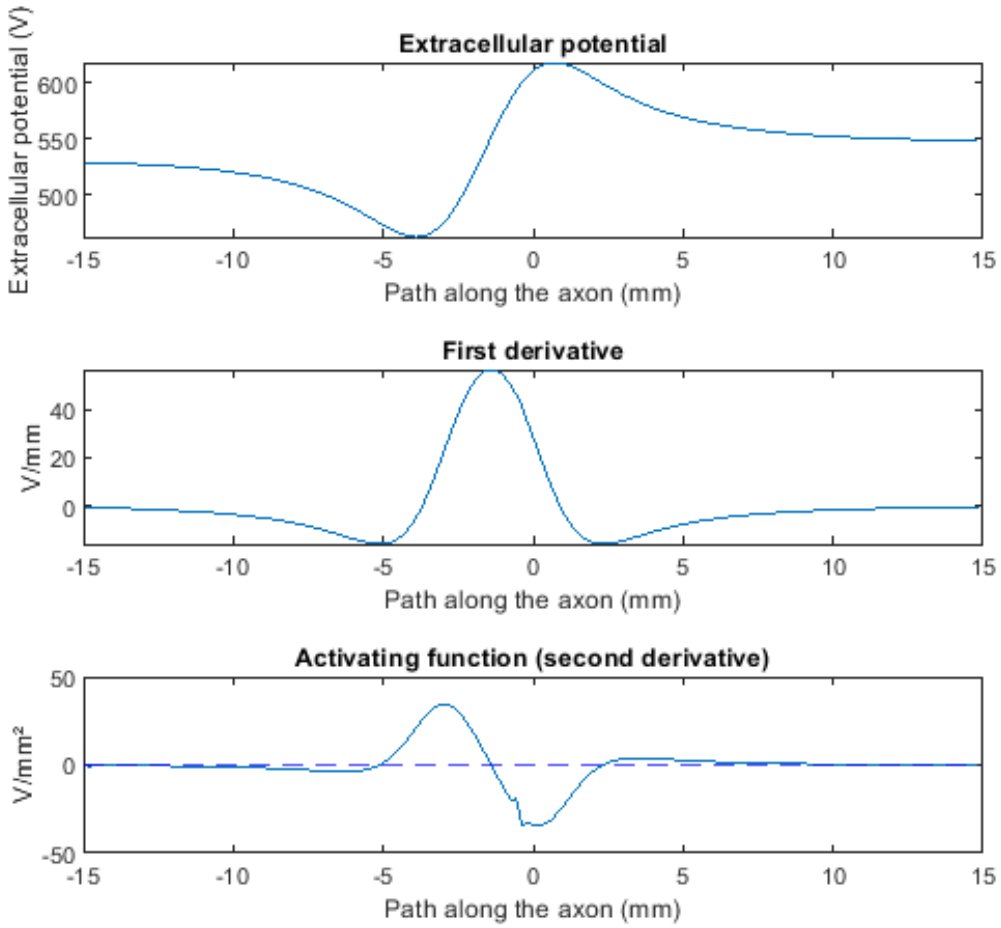

Figure 3.7: The external potential, first derivative and activating function in anodal stimulation of C fibers with the active electrode positioned above the center of the DRG.

3.4.3 Influence of axon location on the excitation threshold of C fibers when stimulated by anodal stimulation

The next step is to look at the influence of the position of the C fiber axon along the Z-axis. The results are shown in Table 3.22 when using a monophasic pulse with a pulse width of 0.1 ms.

Table 3.22: Influence of the position along the Z-axis of C nerve fibers on the time of first spike and the excitation threshold current when subjected to anodal stimulation with a monophasic pulse (pulse width equal to 0.1 ms).

Axon position along the Z-axis (mm)	**Location of first spike (mm)**	**Time of first spike (ms)**	**Excitation threshold current (mA)**
1.090	-3.25	0,493	39,24
0.545	-3.35	0,490	69,48
0.000	-3.45	0,495	115,79
-0.545	-3.60	0,495	183,56
-1.090	-3.75	0,493	281,34

From Table 3.22 it becomes clear that the excitation threshold current is still not within clinical ranges if the axon is located at 1.09 mm along the Z-axis. When the axon is located closest to the electrode the excitation threshold equals 39.24 mA and when the axon is positioned furthest away from the electrode the threshold equals 281.34 mA. This is again an indication that C fibers are not directly stimulated by DRGS according to this model.

3.4.4 Influence of stimulation pulse width and stimulation pulse for anodal stimulation of C fibers

The next parameter that is studied is the pulse width of the modulating pulse. To study this, five values for the pulse width are chosen varying from 0.1 ms to 0.5 ms. The results can be seen in respectively Tables 3.23 to 3.26. Note that the results for a pulse width of 0.1 ms are already shown in Table 3.22.

Table 3.23: Influence of stimulating C fibers with anodal stimulation using a monophasic pulse with a pulse width of 0.2 ms on the location of first spike, time of first spike and excitation threshold current for different positions of the fibers along the Z-axis.

Axon position along the Z-axis (mm)	**Location of first spike (mm)**	**Time of first spike (ms)**	**Excitation threshold current (mA)**
1.090	-3.25	0.563	22.35
0.545	-3.35	0.560	39.54
0.000	-3.45	0.560	66.31
-0.545	-3.60	0.560	105.11
-1.090	-3.75	0.563	160.12

Table 3.24: Influence of stimulating C fibers with anodal stimulation using a monophasic pulse with a pulse width of 0.3 ms on the location of first spike, time of first spike and excitation threshold current for different positions of the fibers along the Z-axis.

Axon position along the Z-axis (mm)	**Location of first spike (mm)**	**Time of first spike (ms)**	**Excitation threshold current (mA)**
1.090	-3.25	0,623	15.35
0.545	-3.35	0,625	27.01
0.000	-3.45	0,628	45.19
-0.545	-3.60	0,628	71.71
-1.090	-3.75	0,623	110.02

Table 3.25: Influence of stimulating C fibers with anodal stimulation using a monophasic pulse with a pulse width of 0.4 ms on the location of first spike, time of first spike and excitation threshold current for different positions of the fibers along the Z-axis.

Axon position along the Z-axis (mm)	**Location of first spike (mm)**	**Time of first spike (ms)**	**Excitation threshold current (mA)**
1.090	-3.25	0.680	11.91
0.545	-3.35	0.683	21.00
0.000	-3.45	0.683	35.12
-0.545	-3.6	0.680	56.00
-1.090	-3.75	0.685	84.97

Table 3.26: Influence of stimulating C fibers with anodal stimulation using a monophasic pulse with a pulse width of 0.5 ms on the location of first spike, time of first spike and excitation threshold current for different positions of the fibers along the Z-axis.

Axon position along the Z-axis (mm)	**Location of first spike (mm)**	**Time of first spike (ms)**	**Excitation threshold current (mA)**
1.090	-3.25	0.7325	9.95
0.545	-3.35	0.7325	17.56
0.000	-3.45	0.73	29.47
-0.545	-3.60	0.7325	46.66
-1.090	-3.75	0.7325	71.22

These results show that when the pulse width of the modulating pulse increases the excitation threshold current will decrease. When using a modulating pulse of 0.5 ms this excitation threshold equals 9.95 mA for the C nerve fiber closest to the electrode which is much lower than 39.24 mA when using a modulating pulse of 0.1 ms. In spite of the fact that this threshold value is lower it's still not within the clinical range of 1 mA.

Subsequently the same trend as for Aβ fibers also occurs regarding the time of first spike. An action potential occurs faster when the pulse width of the modulating pulse is smaller and vice versa.

Next a biphasic pulse with the anodal phase first and second the cathodal phase is applied instead of a monophasic pulse. The results are shown in Table 3.27.

Table 3.27: Influence of stimulating C fibers using a biphasic pulse with first the anodal and second the cathodal phase with a pulse width of 0.1 ms for each phase on the location of first spike, time of first spike and excitation threshold current for different positions of the fibers along the Z-axis.

Axon position along the Z-axis (mm)	**Location of first spike (mm)**	**Time of first spike (ms)**	**Excitation threshold current (mA)**
1.090	-3.30	0,2	151.27
0.545	-3.45	0,2	269.15
0.000	-3.55	0,2	451.86
-0.545	-3.65	0,2	715.12
-1.09	-3.70	0,2	1092.32

From Table 3.27 it becomes clear that the excitation threshold current when the axon is positioned closest to the electrode equals 151.27 mA and the threshold equals 1092.32 mA when the electrode is positioned furthest away from the electrode. Again these values are far from within clinical ranges and will not be used in a clinical setting.

3.4.5 Influence of axon diameter when stimulating C fibers by anodal stimulation

Again the diameter is varied between 0.2 μm and 1.5 μm. The results can be seen in Table 3.28.

Table 3.28: Influence of the axon diameter on the time of first spike and excitation threshold current when performing anodal stimulation on a C fiber positioned in the middle of the DRG using a monophasic pulse with a pulse width of 0.1ms.

Axon diameter (μm)	**Location of first spike (mm)**	**Time of first spike (ms)**	**Excitation threshold current (mA)**
0.2	-3.55	0.495	526.51
0.8	-3.45	0.495	115.79
1.5	-3.45	0.490	71.71

Table 3.28 shows that the excitation threshold current of C fibers decreases when the diameter is increased and vice versa, conform Aβ fibers. These values are still not between clinical values.

3.5 Stimulation of nerve bundles

To optimize the DRGS technique it is important to know how many nerve fibers are activated when a certain stimulation technique is applied. To study this, cathodal stimulation with the cathode above the center of the DRG is performed on a bundle of Aβ nerve fibers. Subsequently the distance of the electrode shaft to the DRG is increased and the excitation thresholds are studied. Cathodal stimulation is chosen because it could be seen that independent of anodal or cathodal stimulation, the location of first spike is the location of the node closest to the cathode. It would be of no value to perform these simulations on C fibers because the model showed that the excitation thresholds of these thin unmyelinated C fibers are not within the clinical range of 1mA if the electrode shaft is located closest to the DRG.

The bundle of nerve fibers consists of 19 Aβ fibers as shown in Figure 3.8.

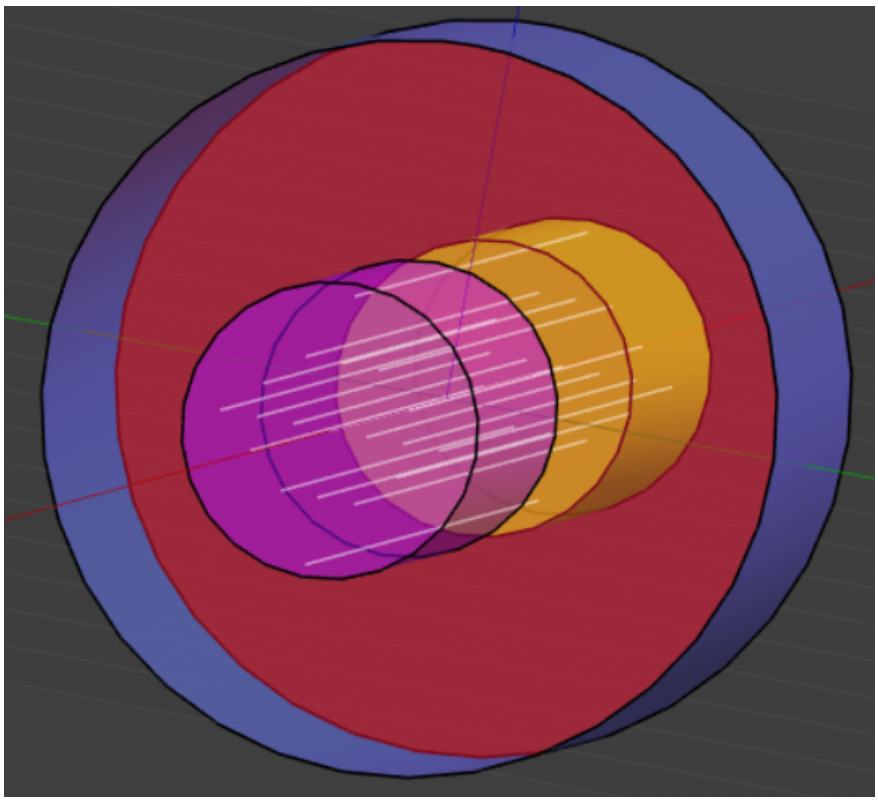

Figure 3.8: Nerve bundle consisting of 19 Aβ nerve fibers located within the DRG.

The location of the straight line axons in the YZ plane are shown in Table 3.29.

Table 3.29: Location of the 19 straight line Aβ fibers in the YZ plane forming a nerve bundle in the DRG.

	Y (mm)	**Z (mm)**
Axon 1	0,0000	1,0900
Axon 2	0,0000	0,5450
Axon 3	0,0000	0,0000
Axon 4	0,0000	-0,5450
Axon 5	0,0000	-1,0900
Axon 6	0,2975	0,0000
Axon 7	0,5950	0,0000
Axon 8	0,8925	0,0000
Axon 9	-0,2975	0,0000
Axon 10	-0,5950	0,0000
Axon 11	-0,8925	0,0000
Axon 12	-0,2975	0,5450
Axon 13	-0,2975	-0,5450
Axon 14	-0,5950	-0,2725
Axon 15	-0,5950	0,2725
Axon 16	0,5950	0,2725
Axon 17	0,5950	-0,2725
Axon 18	0,2975	-0,5450
Axon 19	0,2975	0,5450

The aim is to look at what percentage of nerve fibers is activated by DRGS. To do so the condition for activation has to be defined. In this work is chosen to assume that a nerve fiber with an activation threshold lower than 1 mA is considered activated and a nerve fiber with an activation threshold higher than 1 mA is considered not activated. If, for example, the distance from the center of the active electrode to the center of the DRG is set to 7.65 mm it becomes clear that the percentage of activated nerve fibers equals 63.16% as shown in Table 3.30.

Table 3.30: Percentage of activated Aβ nerve fibers in a nerve bundle consisting of 19 nerve fibers located in the DRG with the distance between the center of the DRG and the center of the active electrode equal to 7.65 mm.

	Activation (yes/no)	**Excitation threshold (mA)**
Axon 1	yes	0,56
Axon 2	yes	0,74
Axon 3	yes	0,96
Axon 4	no	1,24
Axon 5	no	1,56
Axon 6	yes	0,97
Axon 7	yes	0,98
Axon 8	yes	0,98
Axon 9	yes	0,97
Axon 10	yes	0,98
Axon 11	yes	0,98
Axon 12	yes	0,74
Axon 13	no	1,24
Axon 14	no	1,10
Axon 15	yes	0,86
Axon 16	yes	0,86
Axon 17	no	1,10
Axon 18	no	1,24
Axon 19	yes	0,74
% Activated nerve fibers		63,16

To determine the influence of the electrode distance on the percentage of nerve fibers that is activated within the DRG, the activating threshold of the axons in regard to the clinical value of 1 mA is determined for an increasing distance between the center of the electrode and the center of the DRG. The result is shown in Figure 3.9.

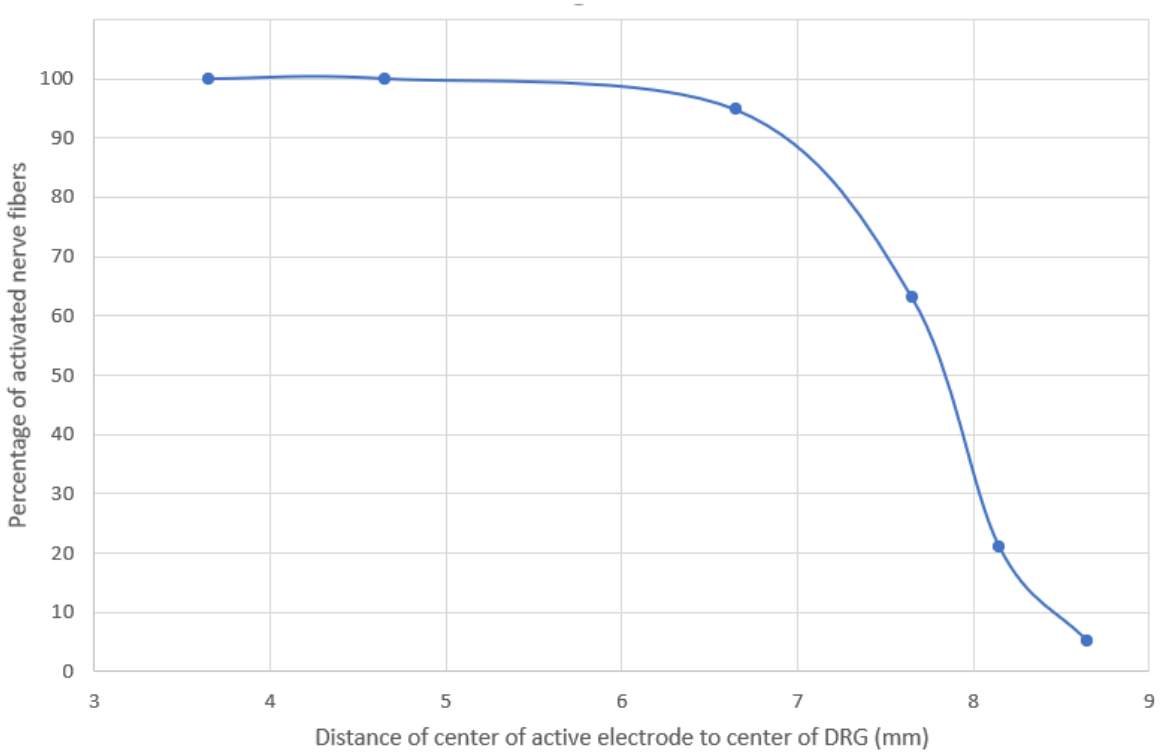

Figure 3.9: Percentage of activated Aβ nerve fibers when subjected to DRGS versus distance between the center of the DRG and the center of the activate electrode.

From this figure it becomes clear that until a distance of 6.65 mm a high percentage of nerve fibers is activated. From this point on increasing the distance results in a steep slope downwards in the curve.

Chapter 4

Discussion

In this chapter the results that were previously generated are discussed.

4.1 Stimulation of Aβ fibers

To start, the results for stimulation of Aβ nerve fibers are discussed and explained where needed. A general note is that the results for cathodal and anodal stimulation are almost the same in every parameter examined. This is due to the fact that in anodal stimulation the only difference is that the anode and cathode are switched. As shown by the activating functions an action potential will arise under the cathode. Subsequently the node closest to the cathode will be activated first and an action potential will arise at this point. Switching the anode and cathode results in a different position of excitation along the axon, but the rest of the electric field doesn't change. The data used in this chapter is extracted from the tables presented in the results chapter.

4.1.1 Effect of changing the axon location and pulse width

When looking at the results concerning the pulse width for different axon positions within the DRG, it becomes clear that if the axon is located further away from the active electrode a higher excitation threshold is observed as shown in Figure 4.1. A quantitative study to these current excitation thresholds could be a first step to determining the ideal stimulation current for chronic pain relief. Figure 4.1 it also shows, as previously mentioned, that the results for cathodal (A) and anodal (B) are similar.

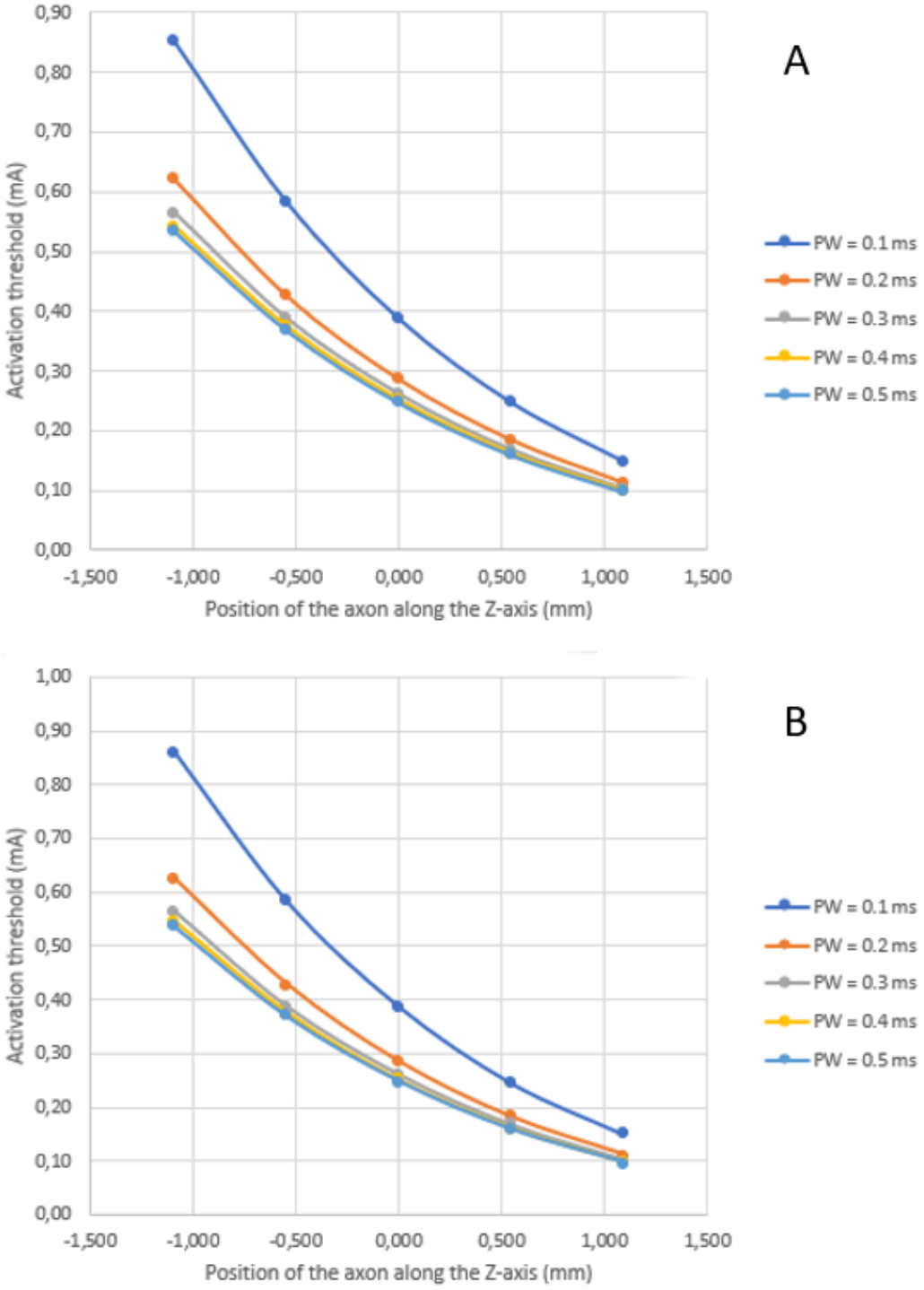

Figure 4.1: Excitation threshold current versus position of the Aβ fiber along the Z-axis for cathodic (A) and anodic stimulation (B) using a monophasic pulse with varying pulse widths.

It can also be seen that if the pulse width increases the activation threshold decreases. This decrease in threshold value is most significant when the pulse width increases from 0.1 to 0.2 ms and is almost negligible when the pulse width increases from 0.3 to

0.5 ms. This indicates that an optimal pulse width could be 0.3 ms because further increase only results in a later time of first spike, as shown in Figure 4.2, and no significant decrease in activating threshold.

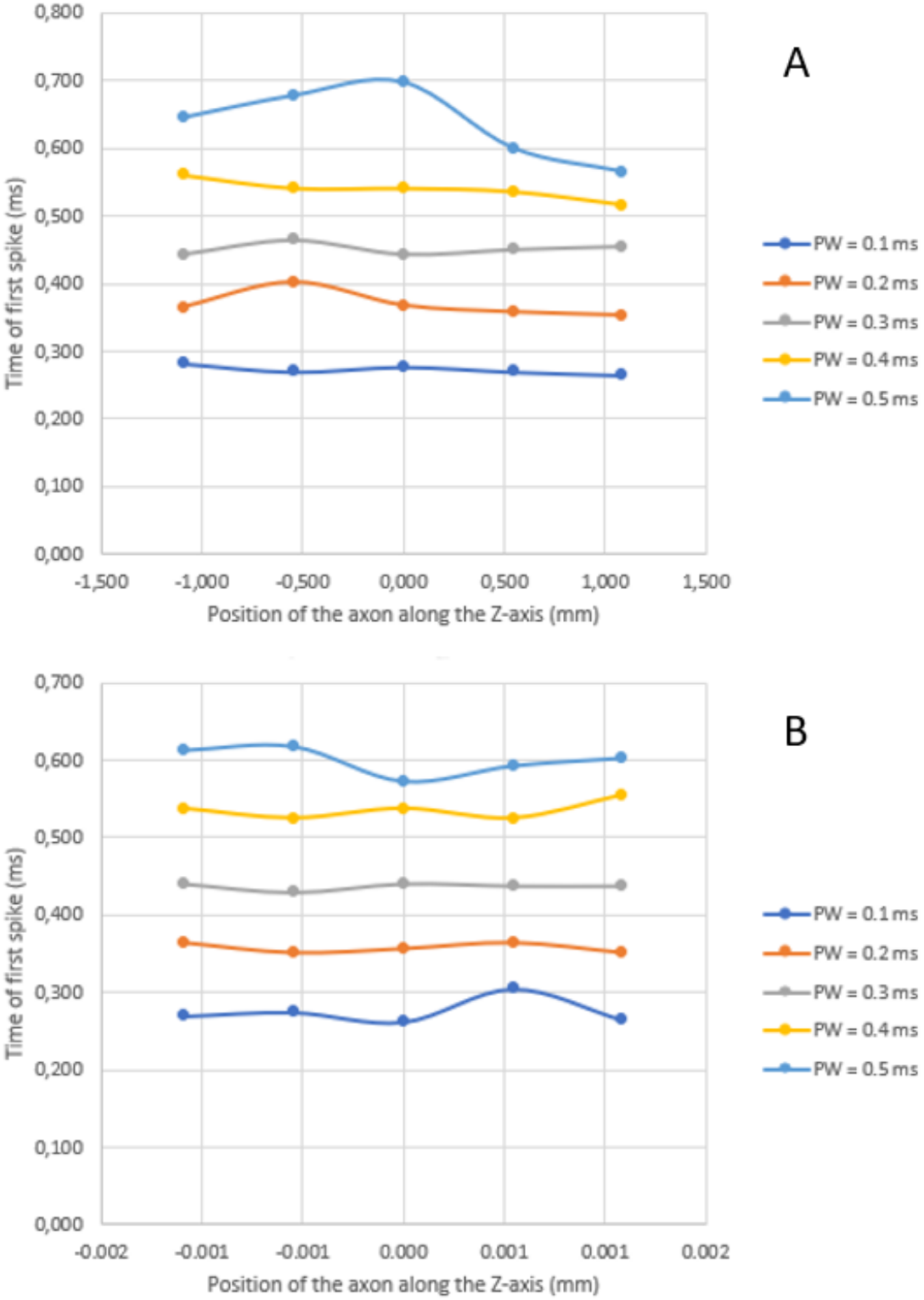

Figure 4.2: Time of first spike versus position of the Aβ fiber along the Z-axis for cathodal (A) and anodal stimulation (B) using a monophasic pulse with varying pulse widths.

Literature shows that SCS activates the large myelinated Aβ fibers, which subse-

quently activates inhibitory interneurons in the dorsal horn (Lempka & Patil, 2018). When using clinical values for the different parameters as done in this study it becomes clear that Aβ fibers are directly activated by DRGS. This could suggest that by activating more Aβ fibers more pain could be relieved. Thus it could be important to set the excitation threshold to such a value that a large amount of Aβ fibers are stimulated.

4.1.2 Effect of varying axon diameter

Thick myelinated Aβ fibers vary in diameter from 5 to 12 μm (Manzano et al., 2008). The influence of this diameter on the excitation threshold current when using anodal and cathodal stimulation of the Aβ fibers is shown in Figure 4.3. Note that these two give the same result as explained in the beginning of this chapter, hence only one plot is made.

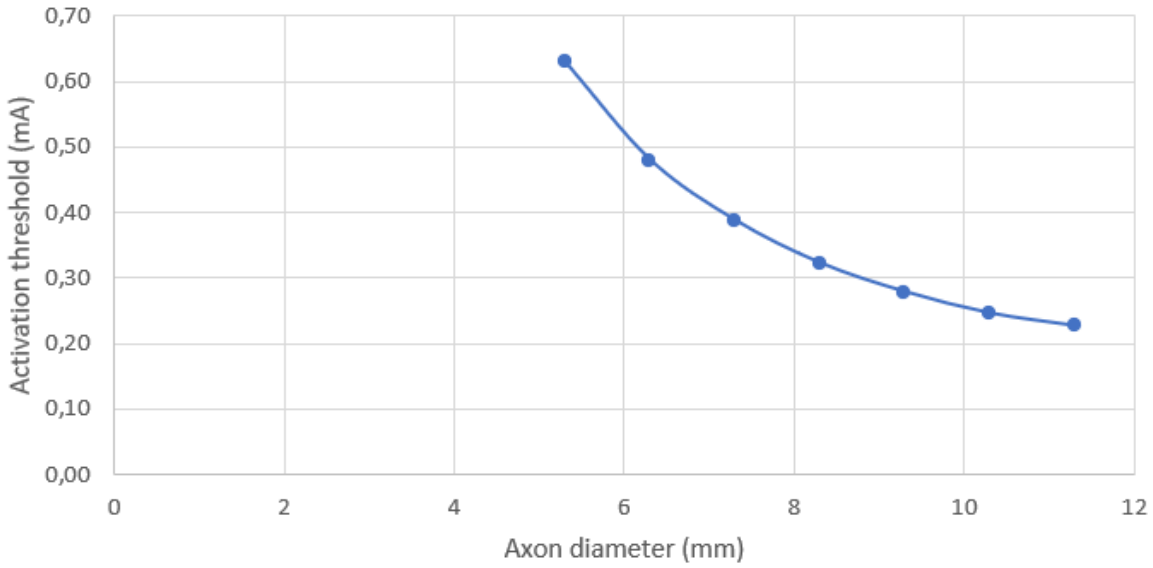

Figure 4.3: Excitation threshold current versus diameter of the Aβ fiber along the Z-axis for cathodal and anodal stimulation when using a monophasic pulse with a pulse width equal to 0.1 ms.

Figure 4.3 shows that the excitation threshold decreases with an increasing axon diameter. This can be explained by looking at the SENN model. The distance between the nodes of Ranvier increases proportional with the diameter as shown in section 2.2.1. Subsequently the potential gradient between the nodes of Ranvier also increases proportional with the diameter. In addition to this the membrane capacitance, proportional with the diameter, and the axial resistance, inversely proportional with the diameter (Equation 4.1), cancel each other out. Equation 4.1 is inversely proportional

with the diameter because L is proportional with the diameter and A is proportional with the diameter squared. Therefore the only mechanism left to influence the relation between threshold and diameter is the distance between the nodes of Ranvier.

$$R_{\mathrm{a}} = r_{\mathrm{i}} \frac{L_{\mathrm{i}}}{A} \tag{4.1}$$

4.1.3 Effect of varying modulation pulse type

In most simulations the modulation pulse is monophasic with a pulse width set to 0.1 ms. To optimise these settings the influence of the pulse type on the stimulation of Aβ fibers is studied. In Figure 4.4 the comparison between the use of a monophasic pulse (blue) to the use of a biphasic pulse (orange) with first the cathodal phase and second the anodal phase is shown. It becomes evident that the excitation threshold is consistently higher when using this biphasic pulse than when using a monophasic pulse.

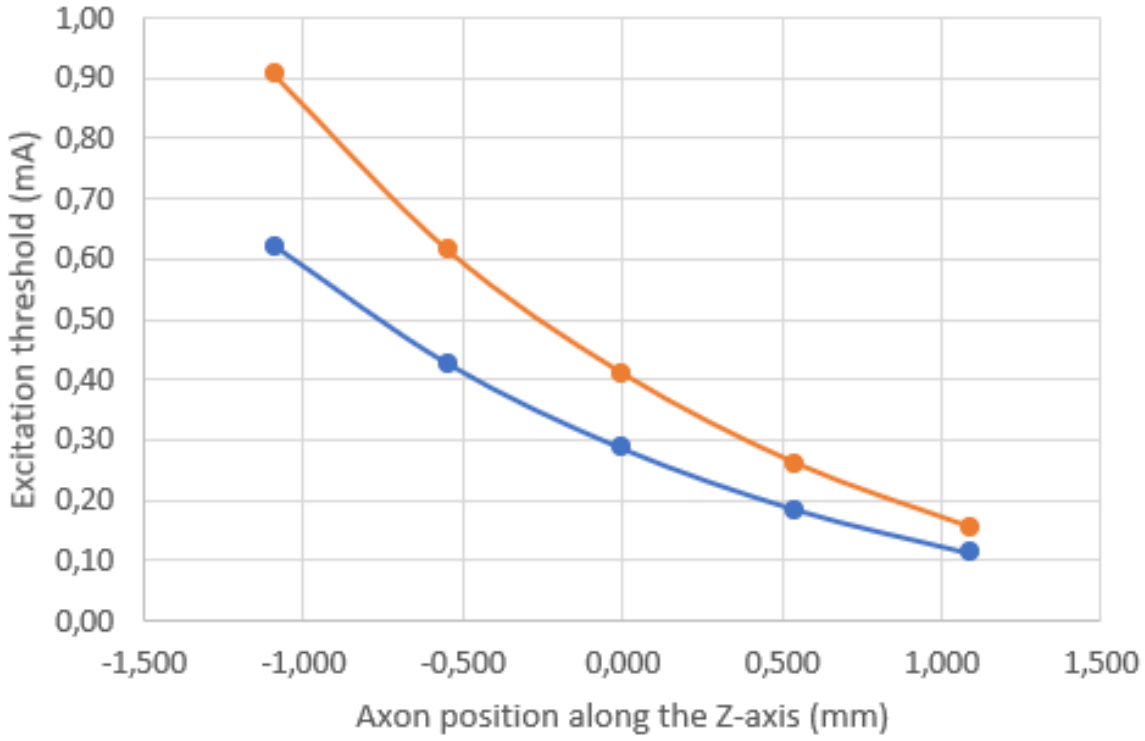

Figure 4.4: Effect of using a monophasic cathodal (blue) versus a biphasic (orange) pulse with first the cathodal phase and than the anodal phase on the excitation threshold along different positions of the Aβ fiber along the Z-axis when using a pulse width equal to 0.1 ms.

This can be explained by looking at the membrane potential plots previously shown in Figure 3.3 for cathodal stimulation and in Figure 3.5 for anodal stimulation. When

first performing cathodal stimulation the depolarization will happen under the active electrode (cathode), when subsequently performing anode-like stimulation hyperpolarization will happen under the active electrode resulting in a less efficient pulse. The same conclusion can be made for anodal stimulation as first phase of the biphasic pulse. In this case hyperpolarization will happen under the active electrode by the anodal stimulation at first followed by depolarization by the cathodal stimulation.

Theoretically the monophasic pulse would be the most efficient pulse, but in practice it is shown that using a monophasic pulse can cause tissue damage (Piallat et al., 2009). When using a biphasic pulse the net charge transfer equals approximately zero (Lilly, 1961). This pulse type is called charge balanced and will not induce tissue damage. The potential of the electrode in the time between pulses (interpulse period) will remain in range resulting in no damaging electrode reactions and no release of noxious products by the electrodes (Cogan, Hara, & Ludwig, 2018). For this reason the biphasic pulse instead of the monophasic pulse is used in clinical settings.

4.2 Stimulation of C fibers

The thin unmyelinated C fibers play an important role in conducting pain as mentioned in section 1.2.2., but the values for the excitation threshold, as determined in section 3.3 and 3.4 are consistently above the clinical value of 0.1 mA (Deer et al., 2017). Even when the pulse width was set to 0.5 ms the value for the excitation threshold was still outside this clinical range. Thus this model suggest that C fibers are not stimulated when using DRGS. Results found in other computational modelling studies came to the same conclusion (Graham et al., 2019).

4.3 Stimulation of a nerve bundle

To optimise the DRGS technique a simulation is performed on a bundle of nerve fibers in order to determine the percentage of nerve fibers that is activated for different positions of the electrode shaft within the foramen. It is known that DRG leads are less prone to positional changes than SCS leads, but the leads could still change location within the intraforaminal space. Studying the effect of this migration could enhance the understanding of what could happen over time in regards to activation of Aβ fibers and could give an indication of in which range the leads could be implanted. Figure 3.9 showed that 94.74% of nerve fibers are activated when the center of the electrode shaft is moved to a distance of 6.65 mm away from the center of the DRG.

Before this point the percentage of activation equaled 100% and after this point the curve shows a steep fall. A lot more data points would be necessary to accurately show the relation between these two factors, but this gives a first indication. According to this model the range in which the leads should be implanted should be between 3.65 and 6.75 mm in terms of distance between the center of the DRG and the center of the electrode shaft.

Chapter 5

Limitations and future work

In this chapter the limitations of the model and future work that still could be done to further understand the behaviour of the nerve fibers involved in DRGS are briefly discussed.

5.1 Neuron morphology

It is important to know the limitations of the model to accurately interpret these results and to understand what could possibly be done in future studies to further optimize the DRGS technique.

The DRG actually consists of pseudo-unipolar neurons. These neurons consist of a soma and a T-junction which bifurcates into a distal and proximal process (Cesmebasi, 2015) as shown in Figure 5.1 (Hordeaux et al., 2020). Unfortunately creating this bifurcation is not possible in Sim4Life, hence straight line axons are used in this model. When using a more accurate representation of the neuron shapes the cathodal and anodal results will differ more because the place of excitation will have more meaning (soma or distal/proximal processes). Naturally bends and other complex shapes will occur. The change in morphology of these neurons will impact the results. Bends can for example create local spots of hypo- or hyper-excitability in response to electrical stimulation (Tranchina & Nicholson, 1986).

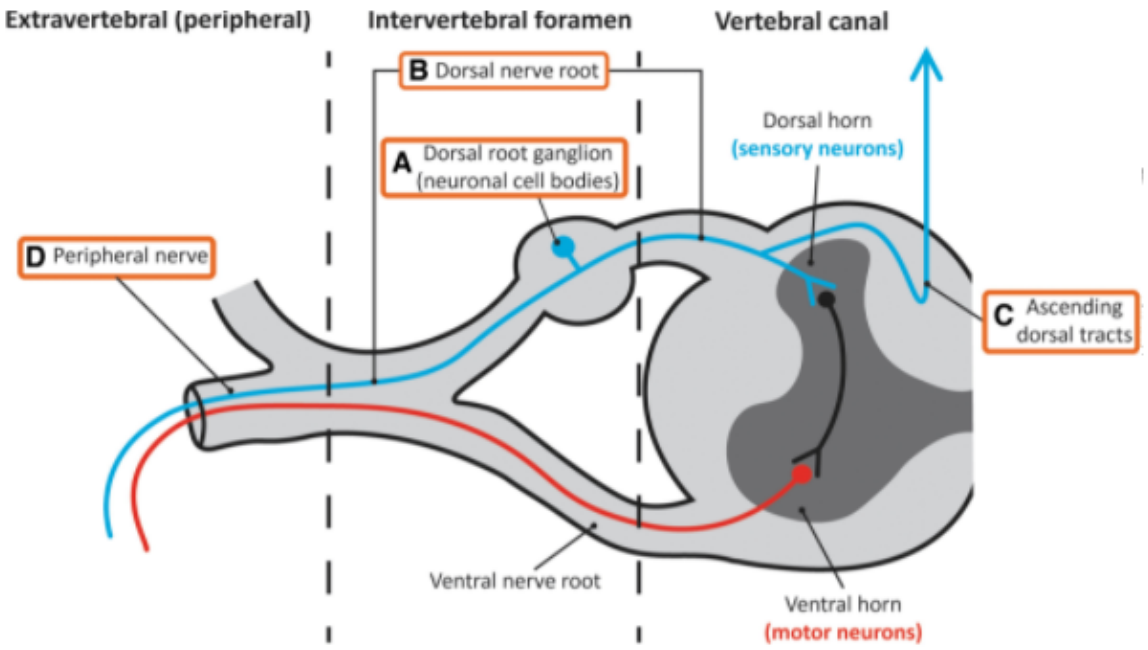

Figure 5.1: Neuroanatomy of the DRG and surrounding structures with (A) the pseudo-unipolar morphology of the neurons in the DRG consisting of a soma and T-junction bifurcating into a distal and proximal process (Hordeaux et al., 2020).

5.2 DRG morphology

The model made in this master dissertation is an ideal cylindrical model as described in section 2.1. The actual morphology of the DRG has a more complex shape as shown in Figure 5.2 (Lin & Chen, 2018).

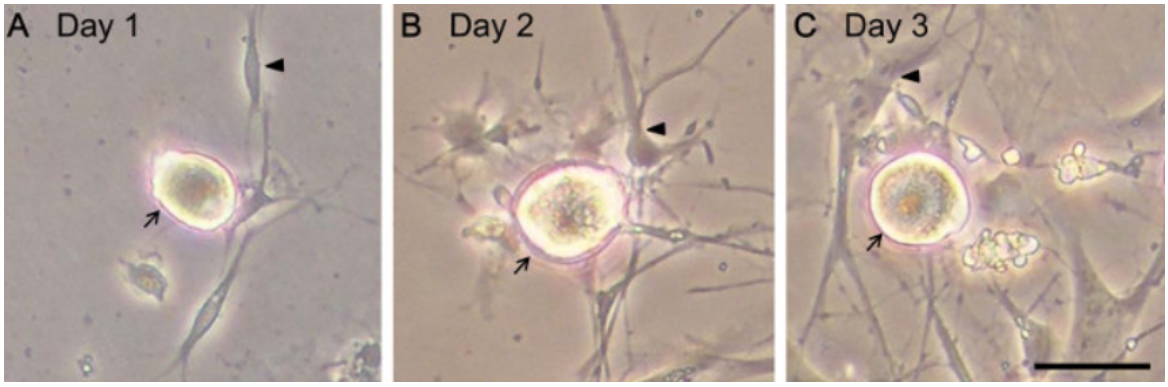

Figure 5.2: Morphology of living DRG cells monitored by microscopy (A) one day after seeding, (B) two days and (C) three days. Arrows indicate neurons and arrowheads indicate glia (Lin et al., 2018).

5.3 Nerve fiber types

In this master dissertation two types of neurons are studied: thick myelinated Aβ fibers and thin unmyelinated C fibers. More nerve fiber types need to be studied to further optimize the DRGS technique. E.g. Aδ fibers which play a role in mechanical and thermal pain (Hu, Cai, Xiao, Luo, & Iannetti, 2014). These Aδ fibers could possibly be stimulated by DRGS since they are myelinated like Aβ fibers, but note that they are thinly myelinated. Thus in future work the impact of DRGS on Aδ fibers should also be researched.

5.4 Electrode types

In this thesis one electrode type is studied: a straight electrode shaft with an active and return electrode (and two inactive electrodes). To further optimize the DRGS technique it could be feasible to research different electrode types.

Chapter 6

Conclusion

In this thesis a model of the DRG is constructed in the software Sim4Life to investigate the behaviour of Aβ and C fibers when subjected to DRGS. The model consisted of the DRG and surrounding layers. Above the DRG a straight electrode shaft was included with the active electrode right above the center of the DRG. Two different nerve fibers were studied: thick myelinated Aβ and thin unmyelinated C fibers. These nerve fibers were modelled by respectively using the SENN and Sundt model. Subsequently a grid study was performed to make the grid as precise as possible while establishing a trade-off between simulation time and accuracy of the results. To automate the process of creating the models, performing simulations and getting results a Python script was written. To further process the data generated with the Python script in Sim4Life two Matlab scripts were created: Activating_Function.m and Membrane_Potential.m. The first Matlab script, Activating_Function.m, plots the extracellular potential, the first derivative and the second derivative (or activating function) of an axon. The second script plots the membrane potential of the axon versus the path along the axon.

Subsequently an analysis was performed. This is done by studying the influence of certain parameters on the behaviour of the neurons when subjected to DRGS. First cathodal and second anodal stimulation of Aβ fibers was performed and the activation threshold was studied. After this the activating function and membrane potential for different time stamps were plotted. The corresponding results showed that the membrane potentials were in accordance to the activating functions.

Thereafter the influence of the axon location along the Z-axis was determined. After studying this it became clear that when the axon position is furthest away from the electrode the excitation threshold was the highest and vice versa. The location of first spike did not change significantly and the first spike was consistently recorded in the

node closest to the cathode. The times of first spike remained in close proximity to each other.

Subsequently the influence of the simulation pulse width and type was examined. By doing so it became evident that the excitation thresholds decreased with an increasing pulse width and vice versa. The decrease in excitation threshold was most significant when varying the pulse width from 0.1 to 0.2 ms and didn't decrease significantly anymore when varying the pulse width from 0.3 to 0.5 ms. The only effect that was observed when increasing the pulse width from 0.3 to 0.5 ms was that the time of first spike increased. Not only the use of monophasic, but also biphasic pulses was studied. The simulations showed that using a biphasic pulse was less efficient than using a monophasic pulse, but because a monophasic pulse could cause tissue damage the biphasic pulse type is used in clinical settings (Piallat et al., 2009).

Finally the influence of the nerve fiber diameter was determined which led to the conclusion that the excitation threshold decreased with an increasing nerve diameter.

After studying the effect of DRGS on Aβ fibers, the C fibers are researched. After stimulating the C fibers with cathodal and anodal stimulation it became clear that the excitation thresholds did not exist between clinical values of DRGS. After performing the same analysis as for Aβ fibers these thresholds were still not within the clinical range of 1 mA. This was a strong indicator that C fibers were not directly stimulated when performing DRGS according to this model.

Finally the influence of moving the electrode shaft further away from the DRG was determined. This was done by looking at the percentage of activated Aβ fibers when performing cathodal stimulation in a nerve bundle consisting of 19 nerve fibers. The results showed that a very high amount of nerve fibers was activated (94.74%) when the center of the electrode shaft was positioned within 6.75 mm away from the center of the DRG. When moving the electrode shaft further away of the DRG the percentage of activated nerve fibers plummeted rapidly.

The general conclusion that can be made with regards to this master dissertation is that with a simple DRG model the behaviour of Aβ and C fibers is assessed when subjected to DRGS. Also shown is that using a monophasic pulse with a pulse width of 0.3 ms is most efficient to activate the Aβ fibers present in the DRG, but the biphasic pulse type is used because the monophasic pulse type could cause tissue damage. In

addition to this it is determined that C fibers are not directly stimulated in DRGS according to the model. Finally the results suggest that most Aβ fibers are activated when positioning the electrode shaft within the range of 6.75 mm center to center distance with respect to the DRG.

References

Ahimsadasan, N., & Kumar, A. (2018). Neuroanatomy, dorsal root ganglion.

Akinrodoye, M. A., & Lui, F. (2020). Neuroanatomy, somatic nervous system. *StatPearls [Internet]*.

Amirdelfan, K., Kramer, J., Cusack, W. F., & Burton, A. W. (2018). Advanced neuromodulation techniques: dorsal root ganglion stimulation. In *Advanced procedures for pain management* (pp. 265–279). Springer.

Andersson, G. B. (1999). Epidemiological features of chronic low-back pain. *The lancet*, *354*(9178), 581–585.

Berta, T., Qadri, Y., Tan, P.-H., & Ji, R.-R. (2017). Targeting dorsal root ganglia and primary sensory neurons for the treatment of chronic pain. *Expert opinion on therapeutic targets*, *21*(7), 695–703.

Borg-Graham, L. (1987). Modelling the somatic electrical behavior of hippocampal pyramidal neurons (msee thesis). *Cambridge, MA: Massachusetts Institute of Technology*.

Breivik, H., Collett, B., Ventafridda, V., Cohen, R., & Gallacher, D. (2006). Survey of chronic pain in europe: prevalence, impact on daily life, and treatment. *European journal of pain*, *10*(4), 287–333.

Brierley, J. (1950). The penetration of particulate matter from the cerebrospinal fluid into the spinal ganglia, peripheral nerves, and perivascular spaces of the central nervous system. *Journal of neurology, neurosurgery, and psychiatry*, *13*(3), 203.

Brodal, P. (2004). *The central nervous system: structure and function*. oxford university Press.

Burgess, P. R., & Perl, E. (1967). Myelinated afferent fibres responding specifically to noxious stimulation of the skin. *The Journal of physiology*, *190*(3), 541–562.

Cesmebasi, A. (2015). Anatomy of the dorsal root ganglion. In *Nerves and nerve injuries* (pp. 471–476). Elsevier.

Cogan, S. F., Hara, S., & Ludwig, K. A. (2018). The safe delivery of electrical currents and neuromodulation. In *Neuromodulation* (pp. 83–94). Elsevier.

Cummins, T. R., Sheets, P. L., & Waxman, S. G. (2007). The roles of sodium channels

in nociception: implications for mechanisms of pain. *Pain*, *131*(3), 243–257.

Dale Purves, D. F. L. C. K. A.-S. L. J. O. M. S. M. W., George J Augustine. (2001). *Neuroscience* (Vol. 2). Sinauer Associates Sunderland, MA.

Deer, T. R., Levy, R. M., Kramer, J., Poree, L., Amirdelfan, K., Grigsby, E., ... others (2017). Dorsal root ganglion stimulation yielded higher treatment success rate for complex regional pain syndrome and causalgia at 3 and 12 months: a randomized comparative trial. *Pain*, *158*(4), 669.

Deer, T. R., Pope, J. E., Lamer, T. J., Grider, J. S., Provenzano, D., Lubenow, T. R., ... others (2019). The neuromodulation appropriateness consensus committee on best practices for dorsal root ganglion stimulation. *Neuromodulation: Technology at the Neural Interface*, *22*(1), 1–35.

Djouhri, L., & Lawson, S. N. (2004). Aβ-fiber nociceptive primary afferent neurons: a review of incidence and properties in relation to other afferent a-fiber neurons in mammals. *Brain research reviews*, *46*(2), 131–145.

Eriksen, J., Sjøgren, P., Bruera, E., Ekholm, O., & Rasmussen, N. K. (2006). Critical issues on opioids in chronic non-cancer pain:: An epidemiological study. *Pain*, *125*(1-2), 172–179.

Erlanger, J., & Gasser, H. S. (1937). Electrical signs of nervous activity.

Esposito, M. F., Malayil, R., Hanes, M., & Deer, T. (2019). Unique characteristics of the dorsal root ganglion as a target for neuromodulation. *Pain Medicine*, *20*(Supplement_1), S23–S30.

Geddes, L. A., & Baker, L. E. (1967). The specific resistance of biological material—a compendium of data for the biomedical engineer and physiologist. *Medical and biological engineering*, *5*(3), 271–293.

Graham, R. D., Bruns, T. M., Duan, B., & Lempka, S. F. (2019). Dorsal root ganglion stimulation for chronic pain modulates a-fiber activity but not c-fiber activity: A computational modeling study. *Clinical Neurophysiology*, *130*(6), 941-951. Retrieved from `https://www.sciencedirect.com/science/article/pii/S1388245719300823` doi: https://doi.org/10.1016/j.clinph.2019.02.016

Grill, W. M., & Mortimer, J. T. (1994). Electrical properties of implant encapsulation tissue. *Annals of biomedical engineering*, *22*(1), 23–33.

Hasegawa, T., Mikawa, Y., Watanabe, R., & An, H. S. (1996). Morphometric analysis of the lumbosacral nerve roots and dorsal root ganglia by magnetic resonance imaging. *Spine*, *21*(9), 1005–1009.

healthline. (2017). Causes of chronic pain.

Hogan, Q. (1996). Size of human lower thoracic and lumbosacral nerve roots. *The Journal of the American Society of Anesthesiologists*, *85*(1), 37–42.

Holsheimer, J. (2002). Which neuronal elements are activated directly by spinal cord stimulation. *Neuromodulation: Technology at the Neural Interface*, *5*(1), 25–31.

Hordeaux, J., Buza, E. L., Dyer, C., Goode, T., Mitchell, T. W., Richman, L., ... others (2020). Adeno-associated virus-induced dorsal root ganglion pathology. *Human Gene Therapy*, *31*(15-16), 808–818.

Hu, L., Cai, M., Xiao, P., Luo, F., & Iannetti, G. (2014). Human brain responses to concomitant stimulation of aδ and c nociceptors. *Journal of Neuroscience*, *34*(34), 11439–11451.

IASP. (2020). Iasp definition of pain.

Kumar, K., Rizvi, S., & Bnurs, S. B. (2011). Spinal cord stimulation is effective in management of complex regional pain syndrome i: fact or fiction. *Neurosurgery*, *69*(3), 566–580.

Leijnse, J. N., & D'Herde, K. (2016). Revisiting the segmental organization of the human spinal cord. *Journal of anatomy*, *229*(3), 384–393.

Lempka, S. F., & Patil, P. G. (2018). Innovations in spinal cord stimulation for pain. *Current opinion in biomedical engineering*, *8*, 51–60.

Lilly, J. C. (1961). Injury and excitation by electric currents. In *Electrical stimulation of the brain* (pp. 60–64). University of Texas Press Austin.

Lin, Y.-T., & Chen, J.-C. (2018). Dorsal root ganglia isolation and primary culture to study neurotransmitter release. *JoVE (Journal of Visualized Experiments)*(140), e57569.

Linderoth, B., & Foreman, R. D. (1999). Physiology of spinal cord stimulation: review and update. *Neuromudulation: Technology at the Neural Interface*, *2*(3), 150–164.

Mai, J. K., & Paxinos, G. (2011). *The human nervous system*. Academic press.

Manzano, G. M., Giuliano, L. M., & Nóbrega, J. A. (2008). A brief historical note on the classification of nerve fibers. *Arquivos de neuro-psiquiatria*, *66*(1), 117–119.

McCorry, L. K. (2007). Physiology of the autonomic nervous system. *American journal of pharmaceutical education*, *71*(4).

Melzack, R., & Wall, P. D. (1996). Pain mechanisms: a new theory: a gate control system modulates sensory input from the skin before it evokes pain perception and response. In *Pain forum* (Vol. 5, pp. 3–11).

Oakley, J. C., & Prager, J. P. (2002). Spinal cord stimulation: mechanisms of action. *Spine*, *27*(22), 2574–2583.

Piallat, B., Chabardès, S., Devergnas, A., Torres, N., Allain, M., Barrat, E., & Benabid, A. L. (2009). Monophasic but not biphasic pulses induce brain tissue damage during monopolar high-frequency deep brain stimulation. *Neurosurgery*,

64(1), 156–163.

Pope, J. E., Deer, T. R., & Kramer, J. (2013). A systematic review: current and future directions of dorsal root ganglion therapeutics to treat chronic pain. *Pain medicine*, *14*(10), 1477–1496.

Poznanski, R. R. (2004). Analytical solutions of the frankenhaeuser-huxley equations i: Minimal model for backpropagation of action potentials in sparsely excitable dendrites. *Journal of integrative neuroscience*, *3*(03), 267–299.

Rattay, F. (1987). Ways to approximate current-distance relations for electrically stimulated fibers. *Journal of theoretical biology*, *125*(3), 339–349.

Reilly, J. P., & Diamant, A. M. (2011). *Electrostimulation: theory, applications, and computational model*. Artech House.

Reina, M., Villanueva, M., López, A., & De Andrés, J. (2007). Grasa dentro de los manguitos durales de las raíces nerviosas de la columna lumbar humana. *Rev Esp Anestesiol Reanim*, *54*(5), 169–72.

Sheets, P. L., Jackson, J. O., Waxman, S. G., Dib-Hajj, S. D., & Cummins, T. R. (2007). A nav1. 7 channel mutation associated with hereditary erythromelalgia contributes to neuronal hyperexcitability and displays reduced lidocaine sensitivity. *The Journal of physiology*, *581*(3), 1019–1031.

Shen, J., Wang, H.-Y., Chen, J.-Y., & Liang, B.-L. (2006). Morphologic analysis of normal human lumbar dorsal root ganglion by 3d mr imaging. *American journal of neuroradiology*, *27*(10), 2098–2103.

Silverstein, M. P., Romrell, L. J., Benzel, E. C., Thompson, N., Griffith, S., & Lieberman, I. H. (2015). Lumbar dorsal root ganglia location: an anatomic and mri assessment. *International journal of spine surgery*, *9*.

Sim4Life. (2020). Sim4life reference guide. In *Sim4life reference guide* (p. 371-372).

Terzis, J. K., & Smith, K. L. (1990). *The peripheral nerve: structure, function, and reconstruction*. Raven Press.

Toblin, R. L., Mack, K. A., Perveen, G., & Paulozzi, L. J. (2011). A population-based survey of chronic pain and its treatment with prescription drugs. *Pain*, *152*(6), 1249–1255.

Toblin, R. L., Paulozzi, L. J., Logan, J. E., Hall, A. J., & Kaplan, J. A. (2010). Mental illness and psychotropic drug use among prescription drug overdose deaths: a medical examiner chart review. *The Journal of clinical psychiatry*, *71*(4), 491–496.

Tranchina, D., & Nicholson, C. (1986). A model for the polarization of neurons by extrinsically applied electric fields. *Biophysical journal*, *50*(6), 1139–1156.

Traub, R. D., Wong, R. K., Miles, R., & Michelson, H. (1991). A model of a ca3

hippocampal pyramidal neuron incorporating voltage-clamp data on intrinsic conductances. *Journal of neurophysiology*, *66*(2), 635–650.

Zelaya, C. E., Dahlhamer, J. M., Lucas, J. W., & Connor, E. M. (2020). Chronic pain and high-impact chronic pain among us adults, 2019.

Znaor, L., Lovrić, S., Hogan, Q., & Sapunar, D. (2007). Association of neural inflammation with hyperalgesia following spinal nerve ligation. *Croatian medical journal*, *48*(1), 35–42.

Appendix A

Ethical aspects and impact of the master dissertation

In this chapter the ethical aspects and impact of the master dissertation are briefly discussed.

This is a computational modelling study, therefore the ethical aspects of the study are rather limited as no interaction with patients or animals has taken place.

The study contributed to a better understanding of the neuronal behaviour when performing dorsal root ganglion stimulation, resulting in information that in time could be a step in the right direction to help doctors to perform DRGS with more accurate implantation in terms of location of the electrodes. This could lead to more and better pain relief.

An ethical downside could be that the device can be hacked and used for bad purposes (similar to hacking a pacemaker).